Review

Advances in Graphene-Based Materials for Metal Ion Sensing and Wastewater Treatment: A Review

Akram Khalajiolyaie and Cuiying Jian *

Department of Mechanical Engineering, York University, Toronto, ON M3J 1P3, Canada; akram70@yorku.ca
* Correspondence: cuiying.jian@lassonde.yorku.ca

Abstract: Graphene-based materials, including graphene oxide (GO) and functionalized derivatives, have demonstrated exceptional potential in addressing environmental challenges related to heavy metal detection and wastewater treatment. This review presents the latest advancements in graphene-based electrochemical and fluorescence sensors, emphasizing their superior sensitivity and selectivity in detecting metal ions, such as Pb^{2+}, Cd^{2+}, and Hg^{2+}, even in complex matrices. The key focus of this review is on the use of molecular dynamics (MD) simulations to understand and predict ion transport through graphene membranes, offering insights into their mechanisms and efficiency in removing contaminants. Particularly, this article reviews the effects of external conditions, pore radius, functionalization, and multilayers on water purification to provide comprehensive insights into filtration membrane design. Functionalized graphene membranes exhibit enhanced ion rejection through tailored electrostatic interactions and size exclusion effects, achieving up to 100% rejection rates for selected heavy metals. Multilayered and hybrid graphene composites further improve filtration performance and structural stability, enabling sustainable, large-scale water purification. However, challenges related to fabrication scalability, environmental impact, and cost remain. This review also highlights the importance of computational approaches and innovative material designs in overcoming these barriers, paving the way for future breakthroughs in graphene-based filtration technologies.

Keywords: molecular dynamics; wastewater treatment; heavy metal pollutants; external field; graphene-based materials

1. Introduction

The global water crisis, driven by rapid industrialization and population growth, has reached alarming levels, leaving 1.2 billion people without access to safe drinking water. This crisis is not merely a matter of scarcity but is compounded by the contamination of water sources, leading to millions of deaths annually from waterborne illnesses [1]. For instance, toxic metals from various sources, including lead, cadmium, and mercury, pose severe risks to both environmental and human health [2,3]. Even at low concentrations, these metals can bioaccumulate in ecosystems and enter the food chain, resulting in long-term health issues [4,5].

The concentration of metals in different wastewater streams varies significantly depending on the type of wastewater and the sources contributing to metal contamination. Industrial effluents, household discharges, and stormwater runoff all contribute to the levels of heavy metals in wastewater. Among the major sources of heavy metal contamination is sewage sludge, a byproduct of wastewater treatment processes. Sewage sludge

accumulates heavy metals from domestic sewage, industrial discharges, and even plumbing systems. Based on this, Table 1 presents the concentration ranges and mean values of selected heavy metals in sewage sludge from municipal wastewater treatment plants, as reported in the work of Spanos et al. [6]. These values are compared with the WHO drinking water guidelines. As can be seen, distinct differences exist between effluent composition and potable water standards, which demands effective heavy metal monitoring and removal.

Table 1. Concentration of heavy metals in sewage sludge [6].

Metal Ion	Range in Sewage Sludge (mg/kg)	WHO Drinking Water Limit (mg/L)
Lead (Pb)	12–102	0.01
Cadmium (Cd)	0.8–7.3	0.003
Copper (Cu)	51–198	2.0
Mercury (Hg)	<0.2	0.006
Zinc (Zn)	810–1880	No health-based limit (<3 for taste)
Chromium (Cr)	13.2–355	0.05 (total Cr)
Hexavalent Chromium (Cr(VI))	0.28–4.3	–

1.1. Heavy Metal Detection

Detecting heavy metals in wastewater is essential for tracking environmental pollution and ensuring water quality. Several methods are employed, each with distinct advantages and limitations. Atomic Absorption Spectroscopy (AAS) [7] is highly sensitive and precise but requires expensive equipment and expertise. Inductively Coupled Plasma Mass Spectrometry (ICP-MS) [8] is extremely sensitive, detecting trace metals at parts-per-trillion levels, though it has high operational costs. X-Ray Fluorescence (XRF) [9] is fast and non-destructive but less sensitive than AAS and ICP-MS. Colorimetric assays [10,11] are simple and useful for on-site testing but have limited accuracy. Neutron Activation Analysis (NAA) [12] is extremely sensitive but requires access to specialized nuclear facilities. UV-Vis Spectrophotometry [13,14] and fluorescence spectroscopy [15] are relatively simple detection methods, with fluorescence spectroscopy providing high sensitivity and selectivity for certain metals. Biosensors [16], which rely on biological molecules, are highly selective but may have varying sensitivity and shorter shelf lives. Electrochemical sensors are portable and cost-effective but struggle with lower sensitivity at very low concentrations [17].

Each method reviewed above serves different purposes based on factors such as cost, sensitivity, and the specific metals to be detected. In wastewater analysis, a combination of selective fluorescence, colorimetric probes, and computational studies can provide a powerful approach for detecting specific heavy metals with high sensitivity and accuracy. For instance, in the case of detecting Hg^{2+} ions, using a benzothiazolinic spiropyran dye offers a practical dual-response system. This dye allows for both a visible color change (from pink to colorless) and a fluorescence signal in the presence of Hg^{2+}, making it possible for quick, on-site detection [18].

1.1.1. Graphene-Based Sensors

With the advancement of functional materials, graphene-based electrochemical sensors have proven highly effective for detecting heavy metal ions in environmental analysis due to their superior sensitivity, selectivity, and portability. When detecting various ions, including mercury and silver, in real water samples, these graphene-based sensors demonstrate high sensitivity and low detection limits, often surpassing conventional methods like ICP-MS [19]. Incorporating nanoparticles can help further enhance performance [20]. For instance, nanocomposites like Nafion–graphene improves detection limits and accuracy for metals such as lead and cadmium [20]. Apart from graphene-based electrochemical

sensors, carbon-based fluorescent materials, especially graphene oxide (GO), offer enhanced stability, biocompatibility, and lower cytotoxicity compared to traditional materials.

A key advantage of GO is its tunable fluorescence, achieved through surface functionalization and size manipulation, enabling visible to near-infrared emissions [21]. Recent studies have demonstrated the high sensitivity and selectivity of GO-based sensors in detecting heavy metal ions, such as Pb^{2+} and Ag^+, leveraging fluorescence quenching and energy transfer mechanisms [22–24]. These sensors excel in water quality monitoring, offering low detection limits and the ability to differentiate between various metal ions, reinforcing GO's potential as a versatile platform for advanced chemical sensing [24–26].

Şenol et al. [27] designed an "off–on" fluorescence sensor for Fe^{3+} based on fluorescein-reduced graphene oxide functionalized with polyethyleneimine. Yu and Zhao [28] developed a competitive fluorescence assay for Cd^{2+} based on aptamer structure-switching. From electrochemical perspectives, Park et al. [29] used graphene oxide as an electrochemically active indicator for detecting Hg^{2+}, and Liu et al. [30] created an electrochemical sensor for ultra-trace Pb^{2+} detection using a nitrogen-doped graphene–gold nanoparticle nanocomposite with ETBD and Fe_3O_4 core–shell nanoparticles. Finally, Tao et al. [31] used silver nanoparticle-decorated graphene oxide for surface-enhanced Raman scattering (SERS), focusing on metal ion detection.

Graphene quantum dots (GQDs) have also been adopted in sensing heavy metal ions. Wang et al. [32] developed a fluorescence sensing platform with GQDs for detecting Cu^{2+}, while Li et al. [33] employed an "on–off–on" fluorescence switch to control cationic interactions. The versatility of graphene-based materials and their ability to be engineered for specific applications highlight their potential as a next-generation sensing platform [19,34]. In the section below, we will review the mechanisms involved in these sensors.

1.1.2. Mechanistic and Bonding Insights into Sensing of Heavy Metals

The interaction between metal ions and graphene-based materials primarily involves coordination bonds, electrostatic interactions, and plasmonic effects, depending on the functionalization and structure. In GQDs, the fluorescence behavior of GQDs is modulated through interactions with metal ions, resulting in either quenching or enhancement [32]. The fluorescence mechanism arises when metal ions like Cu^{2+} or Fe^{3+} interact with GQDs, leading to non-radiative recombination pathways and fluorescence suppression. Fluorescence recovery occurs when these metal ions are displaced by competing molecules or external chemical agents, restoring radiative pathways [33].

In GO-based sensors, their rich oxygen-containing functional groups facilitate electron transfer processes [27,29]. The binding of metal ions such as Hg^{2+} and Fe^{3+} to the surface of GO modifies its electrochemical potential, resulting in a measurable change in current or potential [29]. Reduced GO (rGO) further enhances this effect by improving conductivity and enabling faster electron transport. In the electrochemical detection technique using few-layer GO, heavy metal ions such as Pb^{2+}, Cd^{2+}, and Hg^{2+} adsorb onto the graphene surface through electrostatic interactions, complexation, or π–π interactions with oxygen-containing functional groups ($-COOH$, $-OH$, $-C = O$) [35]. This adsorption alters the charge density and conductivity of graphene, leading to measurable changes in electrical signals [36]. Techniques such as differential pulse voltammetry, square wave voltammetry, and electrochemical impedance spectroscopy detect these signal variations, enabling the precise quantification of metal ions [37]. Measurable electrochemical signals can also be detected via cyclic voltammetry and anodic stripping voltammetry [38,39]. Functionalized electrodes can facilitate redox reactions that generate distinct peaks for specific ions such as Pb^{2+}, Cd^{2+}, and Hg^{2+}, enhancing detection accuracy [40]. Additionally, graphene-based electrodes facilitate anodic stripping voltammetry, where metal ions first undergo electro-

chemical deposition followed by oxidative stripping [41]. Colorimetric detection is another mechanism, where graphene-based nanocomposites induce visible color changes upon binding with heavy metal ions, allowing for a simple and rapid identification method [42]. In the detection of Hg^{2+}, GO forms a stable chelation complex, while the incorporation of fluorescein-functionalized rGO with polyethyleneimine enables a fluorescence mechanism for Fe^{3+} detection, as demonstrated by Senol et al. [27].

Hybrid nanocomposites enhance sensing performance by combining the properties of graphene-based materials with those of nanoparticles and dopants. For example, Liu et al. [30] developed a composite of nitrogen-doped graphene, gold nanoparticles, and Fe_3O_4 core–shell nanoparticles to detect Pb^{2+} ions. This combination of materials provides multiple pathways for electron transfer, increased surface area, and selective adsorption. The nitrogen atoms create electron-rich sites that strongly coordinate with Pb through non-covalent coordination bonds involving lone-pair electron donation. The gold nanoparticles in the composite act as electron mediators, forming transient bonds that facilitate electron transfer during electrochemical sensing. The use of Fe_3O_4 core–shell structures allows for magnetic separation, improving the efficiency and selectivity of the detection process [30]. Aptamer-based competitive fluorescence assays rely on the structure-switching of aptamers upon binding to metal ions, as demonstrated by Yu et al. [28]. In the presence of Cd^{2+} ions, the aptamer undergoes a conformational change, displacing the fluorophore and quenching fluorescence. This competitive displacement mechanism ensures a highly selective response, as the aptamer is specifically designed to bind to Cd^{2+} with high affinity [28].

Besides electrochemical and fluorescence sensing, surface-enhanced Raman scattering platforms utilize plasmonic enhancement to amplify Raman signals at the metal nanoparticle–graphene interface. The silver nanoparticle-decorated GO system developed by Tao et al. [31] generates localized surface plasmon resonance hotspots that significantly enhance the Raman signal upon metal ion adsorption. This approach enables the highly sensitive detection of metal ions, such as Cd^{2+}, by amplifying the weak Raman signals of adsorbed species [31]. Another mechanism in sensing is the use of graphene field-effect transistors, which have emerged as highly sensitive electronic sensors for detecting heavy metal ions such as Pb^{2+}, Hg^{2+}, Cd^{2+}, and As^{3+}. These sensors operate based on charge transfer and doping effects, where metal ion adsorption alters graphene's charge carrier density, causing a measurable shift in the transistor's electrical response [43,44]. Functionalization with thiols ($-SH$), $-COOH$, and peptides enhances selectivity, enabling ultra-detection limits [43,44]. Table 2 summarizes the sensing mechanisms using graphene-based materials.

Table 2. Heavy metal ion sensing using graphene-based materials.

Metal Ion	Graphene-Based Material	Sensing Mechanism	Limit of Detection	Reference
Cu^{2+}	Graphene and graphene oxide	Fluorescence quenching	1.5 Nm	[32]
Al^{3+}	Graphene quantum dots (GQDs)	Fluorescence quenching	10 nM	[33]
Hg^{2+}	Reduced GO	Electrochemical detection	5 pM	[29]
Fe^{3+}	Functionalized GO with amino groups	Colorimetric sensing	0.1 μM	[27]
Pb^{2+}	GO decorated with nanoparticles	Electrochemical sensing	50 nM	[30]
Cd^{2+}	rGO with DNA aptamers	Fluorescence enhancement	2 nM	[28]
Hg^{2+}	GO	Electrochemical sensing	3 μM	[40]
Pb^{2+}	GO decorated with nanoparticles	Electrochemical sensing	0.25 mM	[45]

Table 2. *Cont.*

Metal Ion	Graphene-Based Material	Sensing Mechanism	Limit of Detection	Reference
Ag^+	GO coated with silver nanoparticles	Surface-enhanced Raman spectroscopy (SERS) detection	0.8 pM	[31]
Cd^{2+}	Few-layer GO	Adsorption mechanism	0.978 nM	[35]
Hg^{2+}	Graphene-based nanocomposites	Optical sensing	1 nM	[46]
Pb^{2+}	Metal oxide–GO nanoparticles	Colorimetric sensing	96 μM	[42]
Hg^{2+}	rGO	Electrical detection via charge transfer	4.985 nM	[44]

1.2. Heavy Metal Removal

As the environmental burden of heavy metals continues to grow, the development and implementation of remediation technologies have become increasingly critical. Technologies such as precipitation, flocculation, ion exchange, and electrochemical methods have been deployed to address heavy metal pollution, each offering unique advantages and limitations [47]. Precipitation and flocculation, though easy to implement, are often less effective in achieving complete removal and may introduce secondary pollution due to the generation of chemical residues or sludge that requires further treatment [48]. Ion exchange techniques, while highly efficient in removing specific metals, are often cost-prohibitive, especially on a large scale [49]. Electrochemical methods, despite their high productivity, face significant design and operational challenges such as electrode fouling, high energy consumption, and the need for the precise control of operating conditions to prevent secondary reactions or electrode degradation. Among these technologies, membrane-based separation methods, including ultrafiltration (UF), nanofiltration (NF), and reverse osmosis (RO), have gained widespread use due to their ability to effectively remove heavy metals from contaminated water. However, conventional membranes are plagued by issues such as fouling, low water production rates, and sensitivity to variations in environmental conditions [50,51].

Recent advancements in nanostructured membranes offer a promising solution to these challenges [52], as they employ mechanisms like size exclusion and Donnan electrostatic exclusion [53,54]. These mechanisms rely on precisely engineered nanopores and interlayer distances to achieve an optimal balance between permeability and selectivity [10,12]. Materials such as metal–organic frameworks [55], zeolites [56], ceramics [57], and carbon-based materials including graphene and carbon nanotubes (CNTs) [58] have attracted significant interest due to their high impurity rejection, chemical resistance, and capacity for high fluid flow. Among nanostructured materials, graphene has emerged as a leading candidate for the next generation of membranes. The versatility of graphene, owing to its easily modifiable carbon backbone, has made it a focal point of research in various separation applications [59,60]. Recent efforts have been directed toward functionalizing graphene with chemical groups to create nanopores that enhance its separation capabilities, particularly RO processes in water treatment [61–64]. Below, we will first provide an overview of common synthesizing methods. Then, we will focus on recent advancements in graphene-incorporated membranes for general water treatments to provide broader contexts and in the particular areas of heavy metal removal to highlight specific challenges related to ions.

1.2.1. Common Graphene Composite Synthesis Methods

The synthesis of graphene-based composites involves integrating graphene or its derivatives, such as GO and reduced rGO, with various matrices, including polymers, met-

als, metal–organic framework (MOFs), and ceramics, to enhance their mechanical, electrical, and thermal properties. One widely used approach is a solution-based method, where GO or rGO is dispersed in a solvent and mixed with a matrix material, followed by solvent evaporation or precipitation. This technique is particularly effective in producing uniform graphene distribution within the host material [65,66]. It is widely used in synthesizing polymer and MOF/GO composites [67].

Another effective method for synthesizing polymer–GO composites is in situ polymerization, which involves incorporating graphene or GO into a monomer solution before polymerization [68]. As monomers polymerize, graphene becomes embedded within the polymer structure, forming a well-integrated composite with strong interfacial bonding. Unlike solution mixing, in situ polymerization ensures the better dispersion of graphene in the polymer phase and allows for the creation of tailored nanostructures with controlled properties. Furthermore, this method does not require large amounts of organic solvents, making it an environmentally friendly alternative [68]. Melt mixing is also a widely used method for fabricating graphene-based polymer nanocomposites, where graphene is dispersed within a molten polymer matrix by applying shear forces [69]. In this process, the polymer is heated to its melting temperature, and graphene is added while the mixture is continuously stirred, typically using equipment like extruders. This method is advantageous due to its scalability and cost-effectiveness. However, challenges such as graphene agglomeration and poor compatibility between graphene and the polymer can hinder performance [70].

For high-quality graphene films, chemical vapor deposition (CVD) is a widely used technique for synthesis. CVD is typically used to synthesize high-quality graphene films on metal substrates like Cu and Ni, where a carbon-containing gas decomposes at high temperatures [71]. This method can also be combined with techniques like melt mixing to incorporate graphene films into a polymer matrix. CVD offers the advantage of producing large, continuous graphene sheets with minimal defects, while challenges such as high equipment costs, temperature requirements, and scalability need to be addressed for industrial use [72]. Electrodeposition is another effective technique for applications requiring graphene-based coatings on metal or polymer surfaces. This process involves dispersing graphene in an electrochemical bath and applying voltage to deposit a thin, uniform graphene-based layer on the desired substrate [73].

Beyond coating, for rGO–metal–metal oxide composites, the synthesis process typically involves the reduction of GO using facile chemical or thermal methods, followed by mixing with metal–metal oxide nanoparticles such as Fe_3O_4, MnO_2, TiO_2, and Ag [74,75]. Hydrothermal synthesis facilitates uniform nanoparticle distribution on rGO sheets, while chemical precipitation methods allow for precise control over particle size and composition.

1.2.2. Advancements in Graphene-Incorporated Membrane Technologies in Water Treatments

Graphene-incorporated membranes have emerged as transformative materials in the field of separation technologies, which have significantly improved the efficiency and sustainability of membrane systems, particularly for applications such as water purification, gas separation, and volatile organic compound (VOC) interception [76]. The single-atom-thick carbon structure of graphene imparts extraordinary mechanical strength (approximately 130 GPa tensile strength), a Young's modulus of 1 TPa, [77], and a high thermal conductivity of 3500 W m^{-1} K^{-1} [15], allowing membranes to endure harsh operating conditions without experiencing structural degradation. This resilience extends the lifespan of graphene membranes, reduces operational downtime, and minimizes maintenance costs. In comparison, CNTs have a tensile strength between 13 and 52 GPa and a thermal conductivity ranging around 6000 W/m·K [78]. Polymeric membranes like polyethersulfone

(PES) and polyvinylidene fluoride (PVDF) generally exhibit tensile strengths in the range of 10 to 80 MPa and have thermal conductivities below 0.5 W/m·K, depending on specific formulations and treatments [79].

Recent advancements emphasize the development of hybrid systems that combine graphene with other functional materials to enhance overall performance. Notably, studies such as Alyarnezhad et al.'s [80] demonstrate that the integration of GO nanosheets into polyvinylidene fluoride membranes enhances mechanical strength and porosity, resulting in membranes capable of degrading dyes like methylene blue with a degradation rate exceeding 83%. The work of Keirouz et al. [81] exemplified the successful integration of advanced electrospinning techniques with 2D graphene derivatives to produce defect-free, high-performance membranes. By utilizing a sustainable solvent system containing Cyrene, this study achieved salt rejection rates exceeding 99.84% [81]. Lou et al. [82] explored metal–organic framework (MOF)-wrapped graphene membranes. These membranes maintained a high surface temperature gradient which thus improved photothermal membrane distillation (PMD) processes [82]. In these PMD applications, harnessing solar energy not only minimizes the need for external heating but also increases operation time. The study by Seraj et al. [83] underscored the importance of graphene's large surface area in maximizing porosity and minimizing temperature polarization effects. They demonstrated that graphene-enhanced membranes maintain high flux rates and salt rejection during vacuum membrane distillation without wetting issues, operating for up to 28 h with minimal performance degradation [83]. By leveraging graphene's exceptional photothermal properties, the study of Aquino et al. [84] demonstrated that advanced membranes can be developed to enhance solar-driven water purification and desalination processes. Graphene's versatility extends to dye removal applications. PVDF-GO membranes exhibit superior photocatalytic efficiency under visible light, as demonstrated by Alyarnezhad et al. [80].

1.2.3. Advancements in Heavy Metal Removal by Graphene-Incorporated Composites

Recently, graphene-incorporated membranes have also been applied to the removal of heavy metals. This section provides an overview of recent progress in the synthesis, characterization, and performance of various graphene-based membranes for the removal of different heavy metals.

A MOF/GO composite membrane was developed by combining MOFs with GO nanosheets in the study of Rao et al. [85]. MOFs, known for their high porosity, increased the adsorption sites for metal ions, while the GO nanosheets enhanced mechanical strength and binding efficiency. This membrane was characterized using Field Emission Scanning Electron Microscopy for surface morphology, Fourier Transform Infrared Spectroscopy for chemical interaction analysis, Transmission Electron Microscopy for nanostructure visualization, and Thermogravimetric Analysis for thermal stability assessment. The copper (Cu) concentration in the filtrate was measured using Inductively Coupled Plasma Optical Emission Spectroscopy (ICP-OES). The composite achieved a removal efficiency of over 98%, demonstrating exceptional performance due to its large surface area and functional groups. Additionally, the membrane maintained high performance after multiple filtration cycles, indicating strong reusability. In the work of Zhang et al. [86], a GO–isophorone diisocyanate membrane was synthesized through cross-linking, forming a stable network that enhanced chemical stability and increased the number of binding sites for heavy metals. Characterization techniques included FTIR for chemical bonding, XPS for surface composition, SEM for morphology, contact angle measurements for hydrophilicity, and zeta-potential tests for surface charge analysis. Heavy metal concentrations (Pb, Cu, Cd, and Cr) were measured using Atomic Absorption Spectroscopy (AAS), which provided accurate detection based on light absorption by metal ions. The membrane exhibited removal

efficiencies exceeding 95% for Pb and Cu and significant removal for Cd and Cr. The cross-linked structure also ensured mechanical strength and chemical durability, making the membrane suitable for multi-metal removal. In the work of Shukla et al. [87], a carboxylated GO-incorporated polyphenylsulfone (PPSU) membrane was synthesized by embedding GO COOH nanosheets into a PPSU matrix, enhancing mechanical strength and hydrophilicity. COOH groups provided additional binding sites for metal ions. The membrane was also characterized using ATR-FTIR to confirm the presence of carboxyl groups; Inductively Coupled Plasma Mass Spectrometry was used to measure the concentrations of heavy metals, in which the membrane demonstrated removal efficiencies of 99% for As and Cr and over 97% for Pb and Zn.

Liu et al. [88] fabricated a ceramic-supported GO composite membrane by coating a ceramic support with a composite layer containing GO and attapulgite clay. The clay's high adsorption capacity, combined with the mechanical stability of the ceramic support, resulted in a highly porous and robust structure. Characterization was conducted using SEM for surface visualization, FTIR for bonding analysis, AFM for nanoscale topography, and mercury intrusion porosimetry for pore size distribution. Metal ion concentrations (Cu, Ni, and Pb) were measured using ICP-OES, allowing for simultaneous multi-metal detection. The membrane achieved removal efficiencies of 98% for Cu, 94% for Ni, and 96% for Pb, demonstrating excellent performance due to its interconnected porous network and hydrophilic properties. Zhang et al. [89] functionalized GO with ethylenediamine (EDA), introducing amine ($-NH_2$) groups that acted as chelating sites for metal ions. Modified GO was assembled into a 3D framework with enhanced adsorption capacity and flexibility. Characterization was used to prove the membrane's ability and surface morphology. ICP-OES was used to measure the concentrations of Mg, Pb, Ni, and Zn. The framework demonstrated over 95% removal efficiency for all metal ions, which showed that it is a highly effective framework for dynamic filtration processes. In Table 3, a summary is provided of the experimental studies reviewed above.

Table 3. Experimental studies of heavy metal removal using graphene-based membranes.

Graphene-Based Material	Heavy Metal	Characterization Test	Average Removal Efficiency	References
Metal–organic framework–GO composite	Cu	FESEM, FTIR, TEM, XRD, and TG	90%	[85]
GO–isophorone diisocyanate	Pb, Cu, Cd, and Cr	FTIR, XPS, SEM, contact angle measurements, and zeta-potential tests	72%	[86]
Ceramic-supported GO–attapulgite composite	Cu, Ni, and Pb	SEM, FTIR, XPS, AFM, XRD, and using mercury intrusion pore size analyzer	99%	[88]
Carboxylated GO-incorporated polyphenylsulfone	As, Cr, Pb, and Zn	ATRFTIR, XRD, XPS, AFM, and using SurPASS electrokinetic analyzer (for zeta-potential test)	80%	[87]
GO framework with ethylenediamine	Mg, Pb, Ni, and Zn	X-ray photoelectron spectroscopy, FTIR, FESEM, and AFM	90%	[89]
GO composite	Pb, Ni, and Zn	FESEM, XPS, using SurPASS electrokinetic analyzer (for zeta-potential test), and pore size distribution tests	95%	[90]
Polyethersulfone nanofiltration membrane modified with magnetic GO–metformin hybrid	Cu	AFM, SEM, and contact angle measurements	92%	[91]

The above works highlight the potential of graphene-incorporated composites to be used as filtration membranes. However, as can be seen, the removal efficiency can be as low as 72%. In other words, for metal ion pollutants (the focus of this review) that can be

highly hydrated but are relatively small compared to organic pollutants, special attention must be paid when employing graphene-based materials.

1.3. Surface Functionalization of Graphene for Heavy Metal Detection and Removal

As shown in Sections 1.1 and 1.2, surface modification plays a pivotal role in advancing materials for efficient heavy metal sensing and filtration. Tuning surface properties, such as functional groups, wettability, porosity, and surface charge, improves sensitivity, selectivity, and removal capacity. Here, we provide a brief review in the context of heavy metal detection and removal, and details on graphene pore functionalization will be presented in Section 3.3.

For heavy metal sensing, surface modification enhances the binding affinity of materials to specific metal ions. Functionalization with chemical groups such as thiol ($-SH$), amine ($-NH_2$), and $-COOH$ has proven effective in capturing heavy metals like Pb^{2+}, Hg^{2+}, and Cd^{2+} [19]. These groups form coordinate bonds with metal ions, enabling rapid and selective detection. Advanced sensing platforms also employ nanomaterials such as metal nanoparticles, which provide large surface areas and improved conductivity for enhanced signal transduction [92,93]. Self-assembled monolayers and the covalent attachment of chelating agents further optimize surface interactions, improving detection efficiency and sensitivity even in low-concentration environments [92].

For filtration and removal, surface modification improves the adsorption kinetics and selectivity of membranes and adsorbents. Functionalization with polymeric coatings, MOFs, and carbon-based nanomaterials increases ion capture efficiency by providing abundant active sites [94]. Hydrophilic modifications enhance water flux and reduce fouling, while porous structures increase the surface area for ion adsorption [95,96]. Surface treatments can incorporate specific ligands or ionic groups that can selectively bind to heavy metals, increasing removal efficiency while minimizing interference from competing ions [95,96]. As can be seen, surface engineering helps create multifunctional materials for heavy metal sensing and remediation. In the context of graphene-based filtrations, we will particularly review the effects of functional groups on pore edges (details in Section 3.3).

The above works highlight the potential of graphene to be used as a purification material for heavy metals. This sparks an interest in directly using graphene sheets as filtration membranes in order to achieve 100% heavy metal removal [41,75]. To fully harness the potential of graphene sheets for water treatment, a deep understanding of their properties at the atomic scale is essential since metal ions are comparably smaller than organic molecules. Computational approaches, which have become increasingly important in fields such as energy and medical research, hold significant promise for advancing clean water technologies [97–99]. Tools such as machine learning, Density Functional Theory (DFT), molecular dynamics (MD), and Computational Fluid Dynamics (CFD) are critical for accurate predictions and optimization in material design [100–102]. MD simulations, in particular, are invaluable for analyzing the atomic motions and dynamics of metal ions, making them ideal for investigating graphene-based membranes [100]. Using MD, we can probe various factors, such as graphene layers, pore sizes, and functional groups. By capturing the behavior of these structures at the atomic level, MD helps identify the optimal setup for effective heavy metal removal, thus guiding improvements in membrane design for both high filtration performance and durability.

In the remainder of this review, we will first briefly introduce MD techniques in Section 2 and then focus on the application of MD techniques in studying ion transport through membranes (Section 3). We will first review the effects of external conditions such as pressure and electric fields and then present how pore sizes, shapes, functionalization, and layer arrangements can affect ion transportations. The mechanisms involved

in filtration are then discussed. To enable large-scale applications, we will present environmental and economic assessments, followed by identifying the key challenges in advancing graphene-based membrane filtration techniques. The final conclusions and future directions are given in Section 4.

2. MD Techniques

MD is a computational method that simulates the interactions between atoms or molecules based on Newtonian physics. It models molecular bonds and angles as springs and uses algorithms like SHAKE to maintain the correct atom separations [103]. MD allows for detailed simulations of ionic and molecular motions, surpassing traditional experimental methods that only provide a macroscopic view. MD simulations calculate forces acting on atoms through potential functions that define atom interactions. The positions and velocities of atoms are updated using equations derived from the Verlet method [104]. Additionally, thermodynamic variables like pressure and temperature are controlled using tools such as thermostats and barostats [105]. For instance, the Nose–Hoover thermostat controls temperature by simulating coupling between the system and an imaginary temperature reservoir, while the Nose–Hoover barostat maintains constant pressure by allowing the MD cell to change shape [106]. These techniques help maintain a system's desired thermodynamic state throughout the simulation. The basic algorithm for MD is described in Figure 1.
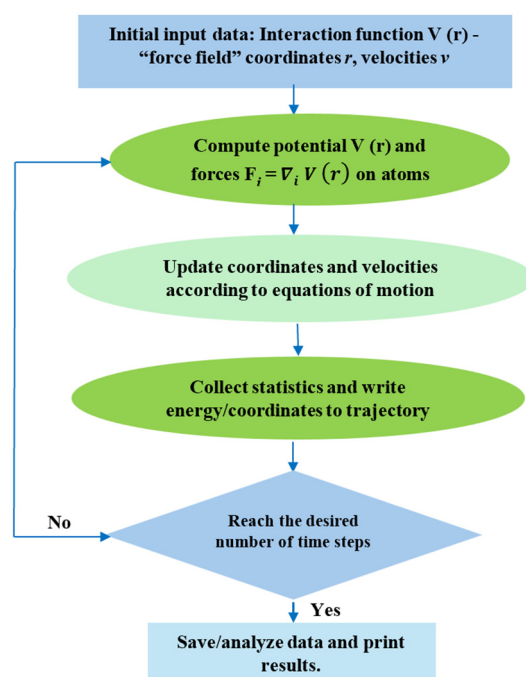

Figure 1. An MD flowchart. MD begins with the definition of initial input data, including interaction potential, the initial coordinates of atoms, and their velocities. Once the system is initialized, potential energy is used to calculate the forces acting on each atom. Next, the positions and velocities of the atoms are updated according to the equations of motion derived from Newton's second law. Throughout the simulation, data such as atomic positions, velocities, and energy values are periodically recorded. The simulation continues until the specified number of time steps is reached.

3. Graphene for Filtration Separations

3.1. Effects of External Conditions

Applying pressure or electrical fields is essential to overcome the energy barriers that naturally restrict ion transport through graphene-based membranes. Pressure in-

creases kinetic energy, reducing energy barriers and facilitating ion passage, while electric fields provide the necessary energy to drive ions through the membrane, particularly when electrostatic interactions create strong repulsion. These external conditions optimize ion rejection and permeability, which enhance membrane performance. In a study by Wang et al. [107], triangular-shaped filtration membranes were subjected to external pressures increasing from 50 to 250 Mpa. In the case of Pb ions filtered through a triangular pore, a high percentage of filtration was achieved within the pressure range of 50 to 150 Mpa. However, at pressures exceeding 150 Mpa, a sharp decline in rejection rates was observed, with the maximum rejection rate dropping to just 60% at 250 Mpa. This reduction may be attributed to excessively high pressures disrupting the interaction between ions and the membrane or accelerating the movement of ions. In contrast, water transport exhibited an upward trend with increasing pressure over time. The pressure range in the study of Kommu et al. [2] varied from 100 to 500 Mpa for graphene pores functionalized with fluorine (F). Meanwhile, at pressures below 500 Mpa, the rejection rate of Co was approximately 100%, and increasing pressure caused a noticeable decline in performance of membrane. The reduction in the energy barrier with increasing pressure confirms that elevated pressure assists ion transport, leading to a decrease in the rejection rate, which dropped to 95% at 500 Mpa. From the perspective of water transport, a linear trend was observed, reaching over 160 molecules per ps per pore, which is 4–5 orders of magnitude higher than those achieved by existing technologies. For graphene functionalized with hydrogen in the work of Khalajiolyaie et al. [108], pressure was applied in the range of 100 to 500 Mpa. The rejection rate of Cd ions from 80 to 350 Mpa was ≥92%, and from 350 to 500 Mpa, a sharp reduction was observed, during which the rejection rate reached around 70%. It was also found that the energy barriers for water transport were higher at lower pressures (15.15 and 14 kJ/mol at 80 and 140 Mpa, respectively) and decreased significantly at higher pressures (6.23 and 3.62 kJ/mol at 420 and 550 Mpa, respectively), indicating that increased pressure facilitates water molecule transport by reducing energy barriers.

Azemat et al. [109] explored fluorinated pores (F-pores) for ion rejection by applying an external electric field to facilitate the transport of Cu^{2+} and Hg^{2+} ions across F-pore membranes. Theis study demonstrated that without the electric field, these ions faced substantial energy barriers. The energy barrier for Hg^{2+} was higher than that for Cu^{2+}, while Cl^- ions were completely blocked due the highest energy barriers. Without an applied electric field, the negatively charged fluorine on the F-pore creates an energy barrier that prevents all Hg^{2+}, Cu^{2+}, and Cl^- ions from passing through the graphene membrane. Under the influence of the electrical field, not only does the passage of water molecules rise significantly, but also ions like Cu^{2+} can permeate the F-pore, overcoming the initial energy threshold of 5 kcal/mol Å. In a study by Majidi et al. [110], γ-graphyne-1 nanosheets functionalized with $-NH_2$ groups were subjected to an electric field ranging from 1 to 8 kcal/mol·Å to investigate the transport of Cu^{2+} and Hg^{2+} ions through the pore area. At less intense electric fields, the ion flux (number of ions per second) was similar for both ions, and the flux increased as the strength of the electric field was raised. However, as the electric field intensified, a significant difference emerged between the number of ions passing through the pores. At an electric field strength of 6 kcal/mol·Å, the ion flux for Cu^{2+} was double that of Hg^{2+} (6 and 3 ions per second, respectively). This difference is attributed to the stronger electrostatic interactions between Hg^{2+} ions and the $-NH_2$ functional groups, which create a higher energy barrier for Hg^{2+} passage compared to Cu^{2+}. Similar results were obtained in the work of Hasanzadeh et al. [111] on Cr(VI) ion permeation through functionalized GO membranes under varying external voltages. It was revealed that ion permeation increases with higher voltages. At lower voltages (0.5–4 kcal/mol·Å), the electric field has minimal impact, and the role of functional groups is more prominent

in influencing ion transport. However, as the voltage rises, ion permeation significantly increases, eventually overshadowing the effects of functional groups. At higher voltages, the dominant factor becomes the electric field, driving more ions through the membrane and reducing the influence of functionalization on the permeation process. In all cases where an electric field is applied as an external condition, increasing the strength of the electric field improves water flux but simultaneously decreases the rejection rate of heavy metals, presenting a challenge in achieving an optimal balance between these two factors. Table 4 summarizes works on the effects of external pressure.

Table 4. Effects of external conditions on heavy metal removal.

Graphene-Based Materials	Pollutant	Average Removal Efficiency	References
Graphene-based materials	Pb^{2+}	$\geq$90% (50–150 MPa), 60% at 250 mPa	[107]
Triangular graphene pores	Co^{2+}	100% (<500 MPa), 95% at 500 MPa	[2]
Graphene functionalized with F	Cd^{2+}	$\geq$92% (80–350 MPa), 70% at 500 MPa	[108]
Graphene functionalized with H	Cu^{2+}, Hg^{2+}	100%	[109]
Fluorinated graphene pores (F-pores)	Cu^{2+}, Hg^{2+}	-	[110]
γ-graphyne-1 functionalized with $-NH_2$	Cr(VI)	Maximum 100%	[111]

3.2. Effects of Pore Sizes and Shapes

In the MD study of Khalajiolyaie et al. [108], simulations were performed on graphene membranes with pore radii of 5, 7, and 10 Å, functionalized with hydrogen (H) or hydroxyl (OH) groups. For H-functionalized membranes, the largest pore radius (10 Å) allowed for significant ion passage due to the lack of interactions between ions and functional groups. With a pore radius of 7 Å, ion rejection was improved, but it still lacked sufficient interaction to prevent passage entirely. In contrast, the smallest pore radius (5 Å) completely blocked ion passage, indicating that the pore was sufficiently small for Cd^{2+} and Cl^- to inhibit their transport. Similar effects of pore sizes were obtained for OH-functionalized membranes. Water flux increased significantly in larger pore areas, with the complete passage of water molecules observed in 10 Å pores. Rahiminejad et al. [112] explored ion rejection in single-layer graphene membranes, examining how nanopore diameters influence the filtration of ions such as Na^{1+}, Ca^{2+}, K^{1+}, Mg^{2+}, and Cl^{1-} from water. The structures of their membranes are shown in Figure 2a. They observed that nanopore size plays a crucial role in balancing water transport and ion rejection. For instance, smaller pores (<15 Å) achieved 100% ion rejection at a pressure of 100 MPa, effectively blocking all tested ions. However, as the nanopore diameter increased to 15 Å, the membrane's ability to reject certain ions, such as K^{1+} and Cl^{1-}, decreased, especially under elevated pressure conditions at 200 MPa. This trend was consistent across intermediate pore sizes of 9–13 Å, where ion rejection efficiency dropped as pore size grew. This study illustrates a clear trade-off: larger pores allow for higher water permeability, facilitating faster flow rates, but they compromise ion rejection efficiency by enabling certain ions to pass through more easily.

The work of Wang et al. [107] optimized the removal of heavy metal ions by embedding graphene sheets with protonated holes of different sizes and shapes using MD simulations. Four types of graphene holes were created: two circular pores with widths of 0.751 and 1.161 nm, a trapezoidal pore, and a triangular pore (Figure 2b). The main focus of their study was to probe how well protonated graphene crown pores remove heavy metal ions such as Cd^{2+}, Cu^{2+}, Hg^{2+}, and Pb^{2+} while maintaining beneficial water permeability. Faster water movement is made possible by larger pores; however, ion rejection may be marginally

compromised. Heavy metal ions encounter greater energy barriers than water molecules, according to free energy calculations, underscoring the capacity of these membranes for selective removal. Also, at the same pressure of 200 MPa for all ions, fewer ions remained on the feed side for triangular pores compared to trapezoidal pore shapes. In a study by Tabasi et al. [113], graphene nanoporous membranes (PGNMs) were utilized to separate As^{3+} and Cu^{2+} ions. Under identical conditions, As^{3+} ions were completely rejected by both small- and large-pore PGNMs, even without functionalization. This indicates that, regardless of functionalization, the size of As^{3+} ions is sufficiently large so that the remaining free space in the pores is insufficient for their passage through these pores. These findings underscore the critical role of ion size in determining transport behavior through both pristine and functionalized membranes. Table 5 shows a summary of the works reviewed in this section.

Table 5. Effects of pore size and shapes on heavy metal removal.

| Graphene-Based Materials	Pollutant	Average Removal Efficiency	References
H-functionalized graphene pores (5 Å)	Cd^{2+}, Cl^-	100% ion rejection	[108]
Nanoporous graphene (<15 Å)	Na^+, Ca^{2+}, K^+, Mg^{2+}, Cl^-	100% ion rejection (at 100 MPa)	[112]
Protonated triangular graphene pores	Cd^{2+}, Cu^{2+}, Hg^{2+}, Pb^{2+}	Fewer ions remain on the feed side compared to other shapes	[107]
Protonated trapezoidal graphene pores	Cd^{2+}, Cu^{2+}, Hg^{2+}, Pb^{2+}	Higher ion passage compared to triangular pores	[107]
Pristine graphene nanoporous membranes (PGNMs)	As^{3+}	100% rejection (even without functionalization)	[113]
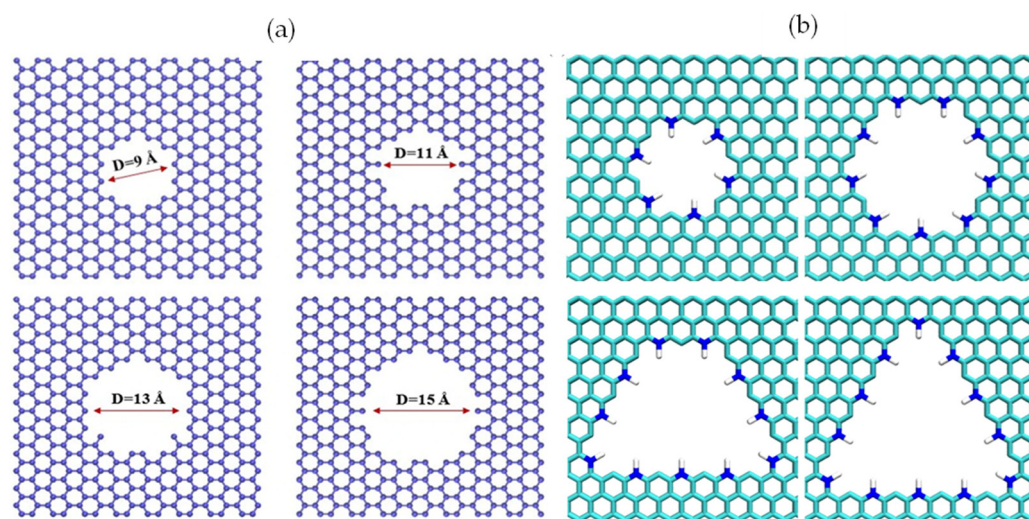
Figure 2. (**a**) Graphene membrane with dimensions of 30×30 Å^2 and different pore diameters 9, 11, 13, and 15 Å. Reprinted from [112], copyright 2022, with permission from Springer Nature. (**b**) Different pore shapes of graphene membrane. Reprinted from [107], copyright 2024, with permission from Elsevier.

3.3. Effects of Functional Groups

In the functionalization of graphene-based materials, two critical factors are considered: the interactions between ions and functional groups and the resulting changes in pore free space. These interactions influence ion transport, as functional groups can either facilitate ion passage through pores or enhance ion rejection, thereby improving purification efficiency. By carefully tuning functionalization, it is possible to optimize the membrane's selectivity and permeability, leading to more effective heavy metal removal. In the study of Khalajiolyaie et al. [108], the ion passage of Cd^{2+} was investigated under identical pressure conditions for H- and OH-functionalized graphene membranes. Detailed analysis revealed

that H-functionalized graphene demonstrated superior performance in rejecting Cd^{2+} ions compared to OH-functionalized graphene. This rejection was attributed to the electrostatic repulsion between the positively charged hydrogen functional groups and the positively charged Cd^{2+} ions. In contrast, Cd^{2+} ions were able to pass through OH-functionalized graphene due to the favorable electrostatic attraction between the oppositely charged OH groups and the Cd^{2+} ions. For the same pore radius with different functionalizations of H and OH, the free space around the pore area was greater in the H-functionalized system compared to the OH-functionalized system. As a result, more water molecules were able to pass through the H-functionalized pore. In the work of Majidi et al. [110], γ-graphyne-1 nanosheets functionalized with $-NH_2$ and $-COOH$ groups at the pore sites were investigated using MD simulations for the separation of Cu^{2+} and Hg^{2+} ions from aqueous solutions. The findings demonstrated that γ-graphyne-1 efficiently separated Cu^{2+} and Hg^{2+} because of its hydrophilic, negatively charged functional groups. $-NH_2$-functionalized γ-graphyne-1 outperformed the $-COOH$-functionalized pores in terms of water passage due to the higher hydrophilicity of $-NH_2$ groups compared to $-COOH$ groups. However, for ion rejection, $-COOH$-functionalized pores yield better results. The reduced hydrophilicity of $-COOH$ groups compared to $-NH_2$ minimized ion transport through the pores, leading to more heavy metals remaining on the feed side. In another study of Zheng et al. [114], the rejection rate of Pb^{2+} ions was investigated for GO membranes functionalized with amino acids. It was found that alanine groups (AlaNeg) led to an increase in the rejection rate, from approximately 30% (for membranes with carboxyl groups) to 80%, representing a 2.67-fold improvement, while there was no huge reduction in water permeability. This enhancement was attributed to strong Coulomb interactions between Pb^{2+} and the negatively charged AlaNeg groups, which formed a dense ionic layer around the functional groups, effectively intercepting Pb^{2+} ions.

Kommu et al. [2] studied salt rejection in nanoporous graphene (NPG) membranes functionalized with hydroxyl (NPG-OH), nitrogen (NPG-N), and fluorine (NPG-F). A graphene sheet (110.55 Å × 106.36 Å) with 25 pores was placed parallel to the xy plane in the simulation. Various heavy metal ions, including $Cd(NO_3)_2$, $Cu(NO_3)_2$, $Pb(NO_3)_2$, $Co(NO_3)_2$, and $Zn(NO_3)_2$, were analyzed for their interactions with functional groups at the pore areas during filtration. At a pressure of 300 MPa, NPG-N- and NPG-F-functionalized membranes exhibited a 100% rejection rate over time for all ions. In contrast, OH-functionalized membranes showed slightly lower rejection rates, ranging from a minimum of 90% for Pb^{2+} to a maximum of 98% for Zn^{2+}. This difference can be attributed to the overall negative charge of the OH group, which can facilitate the passage of positively charged ions due to electrostatic attraction. The rejection rates followed the following order: NPG-N > NPG-F > NPG-OH. While all functional groups possess opposite charges that facilitate ion transfer, the superior performance of NPG-N in terms of rejection rates can be attributed to its stronger electrostatic interactions and higher energy barrier, effectively preventing ion passage. In terms of water permeability, NPG-OH exhibited the lowest water flux due to the reduced free space available around the pores. Moreover, Li et al. [53] simulated ion rejection using three functionalized graphene nanoporous membranes, B-graphene, NH-graphene, and OH-graphene, as shown in Figure 3. Ion rejection was assessed after half of the water molecules passed through the membrane. OH-functionalized graphene achieved 100% ion rejection across all pressures, as the hydrophilic OH groups enhanced water interactions while repelling ions. In contrast, B-functionalized graphene showed decreased ion rejection as pressure increased. While it maintained high rejection (>98%) below 100 Mpa, rejection dropped to above 80% at higher pressures due to weaker hydrophilicity and electrostatic interactions. Increased pressure allowed more ions to pass through, likely due to pore widening and the higher kinetic energy of ions.
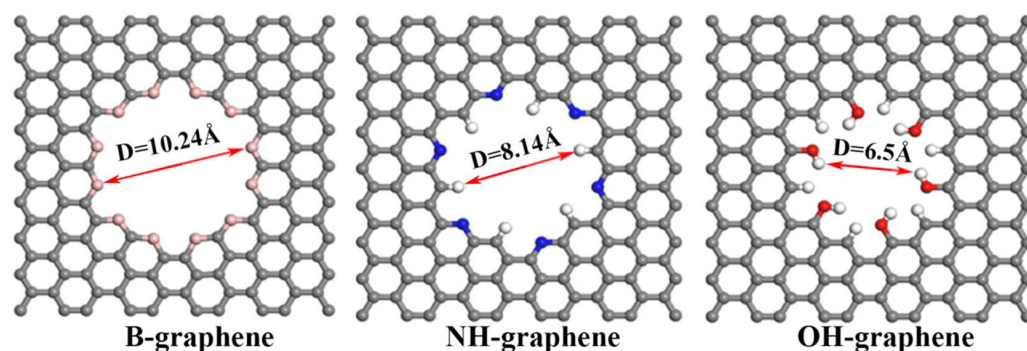
Figure 3. An overhead perspective of three functionalized graphene materials with B, NH, and OH. The membrane's carbon atoms are shown in gray, boron in pink, nitrogen in blue, oxygen in red, and hydrogen in white. Reprinted from [53], copyright 2017, with permission from Elsevier.

Hasanzadeh et al. [111] investigated the permeation of Cr(VI) ions through functionalized GO membranes. At voltages around 3 kcal/mol·Å, the electric field had minimal impact, making the role of functional groups a critical factor in ion permeation. Different functional groups influenced permeation in distinct ways. F-functionalized membranes, carrying a negative charge, attracted positively charged Cr(VI) ions, thereby enhancing ion permeation. In contrast, H- and OH-functionalized membranes, which carry positive charges, exhibited lower efficiency due to reduced electrostatic attraction. However, at high voltages, the influence of functional groups diminished, and pore size became the dominant factor affecting ion transport. Membranes with larger pores, such as those functionalized with F, allowed more ions to pass through, overshadowing the effects of functional groups. Conversely, OH-functionalized membranes, with less free space due to smaller pore sizes, restricted ion passage more effectively. This highlights the interplay between pore size and functionalization in determining ion permeability. The rejection rates of Cu^{2+} ions for both pristine and functionalized PGNMs were investigated by Tabasi et al. [113]. The results show a 100% rejection of Cu^{2+} ions in small-pore PGNMs, regardless of functionalization. For larger pores, functionalization improved Cu^{2+} rejection, with carbamate- and thiourea-functionalized PGNMs achieving the highest rejection rate (approximately 94%), followed by amide- and sulfonic acid-functionalized PGNMs at around 88%. Table 6 presents a summary of the effects of functional groups on heavy metal removal.

Table 6. Effects of functional groups on heavy metal removal.

Graphene-Based Materials	Pollutant	Average Removal Efficiency	References
H- and OH-functionalized graphene	Cd^{2+}	Maximum 98%, 92%	[108]
γ-graphyne-1 with $-NH_2$, COOH functionalization	Cu^{2+}, Hg^{2+}	Moderate ion rejection	[110]
GO membrane with AlaNeg functionalization	Pb^{2+}	Rejection rate increased from 30% to 80%	[114]
NPG-N-functionalized membrane	Cd^{2+}, Cu^{2+}, Pb^{2+}, Co^{2+}, Zn^{2+}	100% for Cd^{2+}, Cu^{2+}, and Co^{2+}; 90% (Pb^{2+}); and 98% (Zn^{2+})	[2]
B-, NH-, and OH-functionalized graphene	Various ions	High rejection (>98%) at low pressure	[53]
Functionalized PGNMs (large pores)	Cu^{2+}	Improved rejection with carbamate and thiourea groups (~94%)	[113]
GO membrane with AlaNeg functionalization	Pb^{2+}	Rejection rate increased from 30% to 80%	[114]

3.4. Effects of Layer Arrangements

While the design of graphene-based membranes with various functionalization and pore geometries is crucial, the study of multilayer structures is equally important. Multilayer configurations are particularly relevant as they more accurately reflect real-world membrane filtration processes. Our recent work [97] evaluated the performance of two-layer graphene membranes functionalized with H and OH groups for water filtration, focusing on pressure, interlayer distance (IS, vertical distance between adjacent layers), and pore alignment [115]. H-functionalized membranes achieved a 100% rejection of Cd^{2+} and Cl^{1-} ions while allowing up to 4000 water molecules to pass, compared to only 45 molecules for OH-functionalized membranes due to stronger hydrogen bonding and a denser structure. MD simulations and statistical modeling showed that increasing pressure and interlayer distance improved water permeability by enhancing the driving force and flow space. A predictive model, validated with a 3% error margin, accurately assessed filtration performance while reducing the need for time-intensive simulations. Compared to fragile, costly, single-layer membranes, bilayer graphene membranes, particularly H-functionalized ones, offer a cost-effective solution for industrial water purification. Zheng et al. [51] studied the impact of offset values (horizontal shift between layers), interlayer spacing (IS, vertical distance between adjacent layers), and gap sizes (width of pores) on metal rejection in layered GO membranes. Increasing the horizontal offset distance between layers significantly enhanced salt rejection. At 50 MPa, an offset of 0.738 nm achieved nearly 100% rejection compared to 80–90% for a 0 nm offset, and this high performance persisted under higher pressures. IS strongly influenced salt rejection, with a smaller IS (0.7 nm) maintaining rates above 80% even at 200 MPa, while a larger IS (0.9 nm) showed a marked decline to 20–30% at the same pressure. Gap size also affected salt rejection, with smaller gaps (0.861 nm) achieving high rates (95%) at lower pressures, but larger gaps exhibited a decline. The study of Zheng et al. [116] examined the effects of nanosheet size, the number of layers, IS, and gap width on the rejection of Cd^{2+} using GO membranes. Two nanosheet sizes were investigated: large nanosheets (LG) with an area of approximately $2.84\,nm^2$ and small nanosheets (SG) with an area with size of $0.75 \times 2.84\,nm^2$, resulting in smaller sheets with more pores per unit area. For membranes composed of identical GO nanosheets, an increase in the number of layers significantly enhanced the rejection rate for Cd^{2+} ions. Membranes with two, three, and four layers showed increasing rejection rates for Cd^{2+}, with the rate exceeding 95% for four-layer SG membranes with a gap width of 1.107 nm and interlayer spacing of 0.7 nm. A smaller interlayer spacing (0.7 nm) provided better retention rates, while wider spacing (0.8 nm) reduced retention rates. For a three-layer membrane with an interlayer spacing of 0.8 nm and a gap width of 1.23 nm, the retention rate increased by 1.22 times. Overall, increasing the number of layers and reducing interlayer spacing increased the energy barrier for Cd^{2+} passage, enhancing the rejection rate and reducing water permeability.

In a further study of Chen et al. [117], GO membranes, with sheet sizes ranging from 20 Å to 50 Å and oxidation degrees of 20% to 40%, demonstrated high heavy metal rejection rates due to tailored structural and chemical features. In this work, oxygen-containing functional groups acted as spacers that reduced interlayer space by forming hydrogen bonds and other molecular interactions (see Figure 4a). Membranes with higher oxidation degrees enhanced rejection, as oxygen-containing functional groups increased surface interactions, leading to denser stacking and restricted ion pathways. Smaller GO sheets improved performance through size exclusion mechanisms, achieving nearly 100% ion rejection, particularly for Pb^{2+} ions. Larger sheets relied on surface interactions within longer interlayer channels, offering slightly lower permeability but still exceeding 95% rejection at high pressures (300 MPa). Water permeability decreased with an increasing

oxidation rate and the number of layers but increased with a larger surface area, as more oxygen groups became exposed on the surface. By combining small-sized sheets with minimized interlayer distances under high assembly pressures, GO membranes can achieve both high ion rejection and efficient water flux.

In the research work of Giri et al. [118], metal ion separation and transport mechanisms in stacked graphene membranes with varying interlayer spacings were investigated (see Figure 4b). For membranes with wider channels, ions like Cd^{2+} and Pb^{2+} have higher permeability due to their second hydration shell behaving like an elastic sphere, allowing water molecules to detach as ions pass through. In contrast, when the first hydration shell is comparable to the channel width, ions cannot pass due to the rigid, tightly bonded structure of the shell, making the membrane highly selective. This underscores the importance of channel dimensions in optimizing membrane performance for specific separation tasks. Metal ions lingered in the channels for extended periods, with over 90% remaining after 100 picoseconds, indicating energetically favorable conditions for ion retention. Water permeance was slightly reduced in membranes with narrower (0.9 nm) channels compared to wider (1.0 nm) ones. The same trend was also observed for metal ions. These findings suggest that narrow channels enhance selectivity and rejection, making them crucial for achieving efficient separation during filtration. The effects of layer arrangements on heavy metal removal are summarized in Table 7.

Table 7. Effects of multiple layers on heavy metal removal.

| Graphene-Based Materials	Pollutant	Average Removal Efficiency	References
H- and OH-functionalized bilayer graphene membrane	Cd^{2+}, Cl^-	100% rejection	[115]
Layered GO membrane with 0.738 nm offset	Salt ions	Nearly 100% rejection at 50 MPa	[51]
Layered GO membrane with 0 nm offset	Salt ions	80–90% rejection at 50 MPa	[51]
Four-layer small GO nanosheets (SG)	Cd^{2+}	>95% rejection with gap width of 1.107 nm and IS of 0.7 nm	[116]
Large GO sheets (>50 Å)	Pb^{2+}	>95% rejection at 300 MPa	[117]
Stacked graphene membranes with narrow channels (0.9 nm)	Cd^{2+}, Pb^{2+}	High selectivity and rejection	[118]
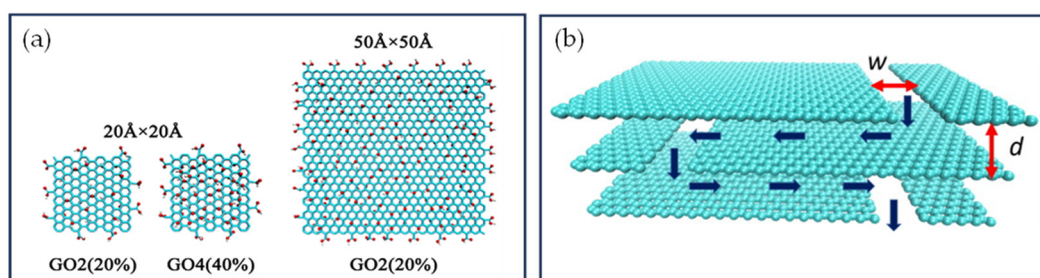
Figure 4. (**a**) The top view of the GO nanosheets utilized in MD simulations, featuring varying oxidation levels and dimensions. Reprinted from [117], copyright 2022, with permission from Elsevier. (**b**) A depiction of multilayer graphene membranes utilized for separating metal ions from solutions. The geometrical parameters, *w* and *d*, represent the width of the channel and the interlayer separation, respectively. The dark blue arrows indicate the solution flow direction. Reprinted from [118], copyright 2021, with permission from Elsevier.

3.5. Mechanistic and Bonding Insights into Heavy Metal

The most common mechanisms in filtration-based heavy metal removal are Donnan electrostatic interactions and size exclusion. The Donnan effect describes the electrostatic exclusion of ions based on a membrane's surface charge. Functionalized graphene membranes, enriched with negatively charged groups such as −COOH and −OH, generate an

electrostatic potential that repels co-ions (e.g., Cl^-) while attracting counter-ions (e.g., Cu^{2+}, Hg^{2+}) [2,109]. This electrostatic attraction increases the local concentration of positively charged heavy metal ions near the membrane surface, facilitating their retention. The presence of $-NH_2$ or $-OH$ groups further reinforces electrostatic binding by these groups acting as electron donors and forming coordination bonds with the metal ions [119]. Size exclusion contributes significantly to the selectivity of graphene-based membranes by filtering ions based on their hydrated radii. Graphene-based membranes have highly tunable nanopore sizes, which can be optimized to permit the passage of water molecules while excluding larger hydrated metal ions. The interplay between Donnan electrostatic interactions and size exclusion ensures that functionalized graphene-based membranes achieve high selectivity and water permeability [120]. This dual mechanism also contributes to the membrane's long-term reusability, as it can prevent membrane clogging and fouling [121]. The enhanced hydrophilicity provided by functional groups, as shown by Lari et al. [122], further promotes water permeability, improving overall filtration performance.

From bonding perspectives, graphene-based membranes achieve heavy metal removal through covalent and non-covalent interactions that regulate ion rejection and water permeability. Covalent bonding occurs when functional groups, such as OH and NH_2, chemically bind to the graphene surface, enhancing ion selectivity and water flux by creating strong hydrogen bonding networks. Lari et al. [122] showed that amino-functionalized GO membranes use covalent bonding to selectively remove Cu^{2+} and Pb^{2+} ions. Non-covalent interactions, such as electrostatic forces, van der Waals interactions, hydrogen bonding, and π-π stacking, further influence membrane performance. Electrostatic interactions arise from charged functional groups on the membrane surface, selectively repelling or attracting metal ions. Azamat et al. [2,109] demonstrated that fluorinated graphene (F-pore) membranes repelled Cl^- ions, while Cu^{2+} and Hg^{2+} ions were transported across the membrane under an external electric field. Zheng et al. [51] reported that GO membranes utilize interlayer van der Waals forces to confine hydrated Cd^{2+} ions while maintaining water permeability. Panahi et al. [119] highlighted that fluorinated carbon nanotubes (FCNTs) facilitate smooth water transport while selectively binding Hg^{2+} ions due to their lower energy barrier compared to Zn^{2+} ions. Li et al. [53] reported that hydroxyl groups form hydrogen bonds with water molecules, reducing the energy barrier for water transport while restricting ion passage due to steric hindrance. In the work of Ercarikci et al. [121], it was found that π-π stacking interactions in graphene membranes stabilize metal ions like Hg^{2+} and Cu^{2+} through aromatic ring interactions.

Beyond Donnan electrostatic interactions and size exclusion mechanisms, chemical adsorption and complexation mechanisms can also play important roles in membrane-based heavy metal removal, with their effects being more prominent in adsorbent-based water purifications. Based on a study by Liu et al. [123], GO functionalized with hyperbranched polyamide-amine (HPAMAM) and microcrystalline cellulose significantly enhances heavy metal adsorption. The complexation mechanism involves metal ions such as Pb^{2+}, Cd^{2+}, and Cu^{2+} binding to nitrogen- and oxygen-containing functional groups on the modified GO surface. $-COOH$, $-OH$, and $-NH_2$ groups present on GO and HPAMAM serve as primary binding sites, forming stable metal ligand complexes through coordination bonding and chelation. Pb^{2+} shows the highest adsorption affinity, forming strong coordination bonds with carboxyl and hydroxyl groups, while Cd^{2+} and Cu^{2+} interact with nitrogen-containing functional groups. The Schiff-based structure introduced further improves metal ion interactions by increasing hydroxyl density and contact area, leading to an increase in adsorption capacities [123].

3.6. Environmental Impact and Life-Cycle Assessments and Recovery and Reutilization of Graphene-Based Materials

While graphene is highly efficient and versatile for heavy metal sensing and removal, for sustainable applications, it is essential to assess the related environmental impacts. An Environmental Impact Assessment (EIA) on graphene production and application in water treatment can raise certain environmental concerns due to high energy consumption and the use of hazardous chemicals [124]. Synthesis methods such as chemical vapor deposition (CVD) and chemical reduction are particularly energy-intensive, while processes like Hummers' method produce toxic byproducts that can contribute to air and water pollution [125]. Environmentally friendly production methods required for scaling in graphene applications. Graphene-based nanomaterials can introduce secondary contamination if not properly managed. Therefore, industrial effluents after purification processes must be properly treated to meet regulatory standards and minimize ecosystem disruption [126,127].

A Life-Cycle Assessment (LCA) provides further insights into the environmental impacts of graphene-based materials from raw material extraction to disposal or recycling. The type and origin of graphite or carbon precursors greatly influence life-cycle impacts. Graphene sourced from renewable carbon feedstocks or waste materials shows reduced environmental burdens compared to mined graphite [128]. The LCA reveals that thermal exfoliation and liquid-phase exfoliation (LPE) have lower environmental impacts compared to CVD and chemical reduction methods, as they require fewer hazardous chemicals and less energy for large-scale production [129,130]. The use of non-toxic solvents and scalable fabrication techniques, such as non-solvent-induced phase separation (NIPS), enhances the sustainability of graphene-based membrane technologies. The incorporation of environmentally friendly solvents, such as triethyl phosphate (TEP), supports scalable and sustainable membrane fabrication, as highlighted in the work of Lou et al. [82]. The findings of Seraj et al. [83] demonstrated that environmentally friendly photothermal membranes fabricated using a solution-casting method, where graphene derivatives were dispersed in a non-toxic solvent to create a homogeneous solution, exhibit high porosity, low wetting propensity, and exceptional thermal stability, supporting sustainable desalination and resource recovery.

The disposal or recycling phase also plays a critical role in preventing environmental contamination. Effective recycling methods, such as filtration and centrifugation, reduce the overall carbon footprint by limiting the need for new material production [129,130]. Once recovered, graphene can be reintegrated into new product formulations or repurposed for secondary applications [126,127,129,130]. Regeneration techniques, such as desorption cycles, can regenerate functionalized graphene after pollutant removal. This reduces the need for fresh graphene production and minimizes waste generation. However, challenges such as incomplete regeneration and chemical degradation during cycles persist.

3.7. Economic Analysis

From an economic perspective, graphene-based electrochemical sensors offer significant long-term cost savings due to their reusability, low maintenance, and ability to provide the real-time monitoring of heavy metal contamination. Despite higher initial costs related to graphene production and sensor fabrication, graphene-based electrochemical sensors could offer significant advantages over traditional laboratory analyses, including real-time, on-site detection; minimal sample preparation; and reusability, which collectively reduce costs and enhance efficiency [131,132]. Their high sensitivity and selectivity could further contribute to their effectiveness in various applications [133]. The economic value of early contamination detection also includes avoiding regulatory fines and preventing environ-

mental damage [134]. Moreover, the incorporation of functionalized nanoparticles and advanced materials such as silver enhances sensor performance but requires optimization to balance costs with performance gains [135].

Similarly, while initial capital investment for graphene membranes is relatively high, their low fouling rates, extended operational life, and energy-efficient filtration could compensate for this over time [136]. For instance, functionalization with hydrophilic groups improves water flux, reducing the energy required for reverse osmosis, thereby making these membranes economically attractive for large-scale applications [4,137]. By integrating dual-mode detection and filtration systems, contamination monitoring and remediation processes could be streamlined, minimizing the need for separate systems and further reducing operational costs [138]. Nevertheless, developing scalable methods to produce defect-free graphene is essential to make graphene-based membranes more economically appealing.

3.8. Challenges

Despite the reviewed advancements, using MD to study nanocarbon-based filtration faces significant challenges. These challenges include the high computational demands required to simulate millions of atoms over numerous time steps, limited timescales that restrict the study of slower processes like large-scale structural changes, and sensitivity to the accuracy of force fields, which approximate interatomic interactions and directly affect the reliability of the results [119,139,140]. These challenges further hinder investigations into the interrelations between membrane characteristics (e.g., pore size, functionalization, number of layers) and external factors such as pressure and electric fields, which are crucial for optimizing membrane performance under diverse environmental conditions.

As mentioned in Section 3.7, the initial cost of graphene-based sensors and membranes is relatively high. Indeed, the large-scale adoption of graphene-based membranes is hindered by high production costs due to complex synthesis methods. Furthermore, material inconsistencies and structural defects (e.g., cracks) induce brittleness and reduce membrane integrity under high pressure, which compromises durability in industrial applications [141]. More importantly, as reviewed above, structural characteristics are also crucial for optimizing the performance of carbon-based membranes in water purification. For instance, the alignment of carbon-based materials is essential for enhancing selectivity and permeability in filtration processes. Additionally, controlling pore sizes at nanoscales is crucial to achieving high ion rejection rates. However, controlling length scales during synthesis and fabrication remains a highly complex task. While recently, emerging sustainable strategies, such as using laser-based manufacturing, offer promising solutions for reducing chemical usage and energy demands [142,143], it is still challenging to obtain defect-free graphene with well-defined pore sizes and layer arrangements. These production difficulties, along with fouling and maintenance requirements induced by material defects, have limited the large-scale integration of these materials into commercial membrane technologies [144].

4. Conclusions and Outlooks

This review highlights the advancements and challenges in the application of graphene-based membranes for ion filtration, with a focus on the effects of external conditions, pore sizes and shapes, functionalization, and multilayer structures. The remarkable progress in graphene-based materials, particularly GO and its derivatives, has unlocked significant potential for metal ion detection and wastewater treatment due to their exceptional properties, such as high surface area, excellent thermal and electrical conductivity, and versatile chemical functionalization. These attributes make graphene membranes highly ef-

fective and selective in filtration applications while supporting sustainable and eco-friendly solutions that reduce energy consumption and minimize reliance on harmful chemicals.

MD simulations provided critical insights into the mechanisms governing ion transport and rejection under varying pressures, electric fields, and functionalization strategies. The studies reviewed demonstrate that external factors such as pressure and electric fields significantly influence filtration performance, with optimized ranges enhancing ion rejection but extreme conditions leading to reduced efficiency. Pore sizes and shapes play a pivotal role in balancing ion rejection and water permeability, with smaller pores favoring higher rejection rates but potentially limiting water flux. The functionalization of graphene membranes emerges as a key strategy to enhance selectivity and filtration efficiency. Functional groups such as $-NH_2$, $-OH$, and fluorine provide tailored interactions with ions, allowing for the selective rejection of specific heavy metals. Multilayer graphene and GO membranes further improve filtration by leveraging interlayer spacing and sheet alignment to achieve superior retention rates and structural stability.

Future work should address challenges in graphene-based membrane development by combining efforts in advanced computational methods and material innovation. Developing and implementing advanced algorithms, enhanced computing power, and precise interatomic potentials will help reduce computational demands, with techniques like parallel processing and machine learning-based approaches accelerating simulations and improving accuracy. Utilizing data regression and correlation analyses, further research is needed to investigate the interplays among pore size, functionalization, and external factors such as pressure and electric fields to optimize membrane performance under diverse environmental conditions. Additionally, new fabrication methods and innovative material combinations should be explored to enhance structural integrity, addressing issues like brittleness and defects. Efforts should also be focused on designing multifunctional graphene membranes capable of simultaneously removing heavy metals, organic pollutants, and other hazardous substances. Finally, to address practical challenges, including scalability, production costs, and long-term durability, developing cost-effective synthesis techniques and combining graphene with other resilient materials could offer promising solutions.

Author Contributions: A.K.: Conceptualization, Investigation, and Writing—original draft. C.J.: Funding acquisition, Methodology, Project administration, Resources, Writing—Review and editing, and Supervision. All authors have read and agreed to the published version of the manuscript.

Data Availability Statement: No new data were created or analyzed in this study. Data sharing is not applicable to this article.

Conflicts of Interest: The authors declare no conflict of interest.

References

1. Geim, A.K. Graphene: Status and Prospects. *Logo* **2009**, *324*, 1529–1534. [CrossRef] [PubMed]
2. Kommu, A.; Namsani, S.; Singh, J.K. Removal of heavy metal ions using functionalized graphene membranes: A molecular dynamics study. *RSC Adv.* **2016**, *6*, 63190–63199. [CrossRef]
3. Katsnelson, M.I. Graphene: Carbon in two dimensions A two-dimensional form of carbon. *Materialtoday* **2007**, *10*, 20–28.
4. Liu, G.; Ye, H.; Li, A.; Zhu, C.; Jiang, H.; Liu, Y.; Han, K.; Zhou, Y. Graphene oxide for high-efficiency separation membranes: Role of electrostatic interactions. *Carbon N. Y.* **2016**, *110*, 56–61. [CrossRef]
5. Azamat, J.; Sardroodi, J.J.; Poursoltani, L.; Jahanshahi, D. Functionalized boron nitride nanosheet as a membrane for removal of Pb^{2+} and Cd^{2+} ions from aqueous solution. *J. Mol. Liq.* **2021**, *321*, 1149–1158. [CrossRef]

6.   Spanos, T.; Karadjova, I.; Ene, A.; Karadjova, I. Assessment of Toxic Elements Cu, Cr, Ni, Pb, Cd, Hg, Zn, As and Hexavalent Chromium in Sewage Sludge from Municipal Wastewater Treatment Plants by Combined Spectroscopic Techniques and Hexavalent Chromium in Sewage Sludge from Municipal Wastewater Treatment Plants by Combined Spectroscopic Techniques. *Artic. Rom. J. Phys.* **2015**, *60*, 237–240.

7.   Abrham, F.; Gholap, A.V. Analysis of heavy metal concentration in some vegetables using atomic absorption spectroscopy. *Pollution* **2021**, *7*, 205–216.

8.   Kopru, S.; Soylak, M. Inductively coupled plasma-mass spectrometry (ICP-MS) detection of trace metal contents of children cosmetics. *Opt. Quantum. Electron.* **2024**, *56*, 399–419. [CrossRef]

9.   O'Neil, G.D.; Newton, M.E.; Macpherson, J.V. Direct identification and analysis of heavy metals in solution (Hg, Cu, Pb, Zn, Ni) by use of in situ electrochemical X-ray fluorescence. *Anal. Chem.* **2015**, *87*, 4933–4940. [CrossRef]

10. Chen, Z.; Zhang, Z.; Qi, J.; You, J.; Ma, J.; Chen, L. Colorimetric detection of heavy metal ions with various chromogenic materials: Strategies and applications. *J. Hazard. Mater.* **2023**, *441*, 129889. [CrossRef]

11. Wu, J.; Li, M.; Tang, H.; Su, J.; He, M.; Chen, G.; Guan, L.; Tian, J. Portable paper sensors for the detection of heavy metals based on light transmission-improved quantification of colorimetric assays. *Analyst* **2019**, *144*, 6382–6390. [CrossRef] [PubMed]

12. Das, D.D.; Sharma, N.; Chawla, P.A. Neutron Activation Analysis: An Excellent Nondestructive Analytical Technique for Trace Metal Analysis. *Crit. Rev. Anal. Chem.* **2023**, *54*, 2450–2466. [CrossRef] [PubMed]

13. José Barreto, W.; Regina Giancoli Barreto, S. Determination of ni(ii) in Metal Alloys by Spectrophotometry Uv-Vis Using Dopasemiquinone. *Quim. Nova* **2010**, *33*, 109–113. [CrossRef]

14. Heffron, J.; Samsami, M.; Juedemann, S.; Lavin, J.; Tavakoli Nick, S.; Kieke, B.; Mayer, B. Mitigation of viruses of concern and bacteriophage surrogates via common unit processes for water reuse: A meta-analysis. *Water Res.* **2024**, *252*, 121242. [CrossRef] [PubMed]

15. Prestel, H.; Gahr, A.; Niessner, R. Detection of heavy metals in water by fluorescence spectroscopy: On the way to a suitable sensor system. *Fresenius J. Anal. Chem.* **2000**, *368*, 182–191. [CrossRef]

16. Verma, N.; Singh, M. Biosensors for heavy metals. *BioMetals* **2005**, *18*, 121–129. [CrossRef] [PubMed]

17. Zhu, C.; Yang, G.; Li, H.; Du, D.; Lin, Y. Electrochemical sensors and biosensors based on nanomaterials and nanostructures. *Anal. Chem.* **2015**, *87*, 230–249. [CrossRef] [PubMed]

18. Ekrami, E.; Pouresmaieli, M.; Shariati, P.; Mahmoudifard, M. A review on designing biosensors for the detection of trace metals. *Appl. Geochem.* **2021**, *127*, 104902. [CrossRef]

19. Chang, J.; Zhou, G.; Christensen, E.R.; Heideman, R.; Chen, J. Graphene-based sensors for detection of heavy metals in water: A review Chemosensors and Chemoreception. *Anal. Bioanal. Chem.* **2014**, *406*, 3957–3975. [CrossRef] [PubMed]

20. Li, J.; Guo, S.; Zhai, Y.; Wang, E. High-sensitivity determination of lead and cadmium based on the Nafion-graphene composite film. *Anal. Chim. Acta* **2009**, *649*, 196–201. [CrossRef] [PubMed]

21. Zhang, H.; Zhang, H.; Aldalbahi, A.; Zuo, X.; Fan, C.; Mi, X. Fluorescent biosensors enabled by graphene and graphene oxide. *Biosens. Bioelectron.* **2017**, *89*, 96–106. [CrossRef] [PubMed]

22. Qu, Y.; Yakub, I.; Baini, R.; Hu, W.; Wang, L. Ag+ colorimetric sensor based on graphene oxide/nano-platinum composite. *J. Anal. Sci. Technol.* **2023**, *14*, 35. [CrossRef]

23. Pathak, P.; Cho, H.J. Graphene Oxide-Chitosan Composite-Based Flexible Electrochemical Sensors for Lead ION Detection. In Proceedings of the 21st International Conference on Solid-State Sensors, Actuators and Microsystems, TRANSDUCERS 2021, Orlando, FL, USA, 20–24 June 2021; pp. 254–258.

24. Wang, Z.; Yao, B.; Xiao, Y.; Tian, X.; Wang, Y. Fluorescent Quantum Dots and Its Composites for Highly Sensitive Detection of Heavy Metal Ions and Pesticide Residues: A Review. *Chemosensors* **2023**, *11*, 405. [CrossRef]

25. Li, X.; Wang, G.; Ding, X.; Chen, Y.; Gou, Y.; Lu, Y. A 'turn-on' fluorescent sensor for detection of Pb^{2+} based on graphene oxide and G-quadruplex DNA. *Phys. Chem. Chem. Phys.* **2013**, *15*, 12800–12804. [CrossRef]

26. Barzegarzadeh, M.; Amini-Fazl, M.S.; Yazdi-Amirkhiz, S.Y. Polymethacrylamide-functionalized graphene oxide via the RAFT method: An efficient fluorescent nanosensor for heavy metals detection in aqueous media. *Chem. Pap.* **2022**, *76*, 4523–4530. [CrossRef]

27. Şenol, A.M.; Onganer, Y.; Meral, K. An unusual "off-on" fluorescence sensor for iron(III) detection based on fluorescein–reduced graphene oxide functionalized with polyethyleneimine. *Sens. Actuators B Chem.* **2017**, *239*, 343–351. [CrossRef]

28. Yu, H.; Zhao, Q. Competitive fluorescence assay for Cd2+ based on aptamer structure-switching. *Microchem. J.* **2023**, *194*, 109348. [CrossRef]

29. Park, H.; Hwang, S.J.; Kim, K. An electrochemical detection of Hg2+ ion using graphene oxide as an electrochemically active indicator. *ElectroChem. Commun.* **2012**, *24*, 100–103. [CrossRef]

30. Liu, F.M.; Zhang, Y.; Yin, W.; Hou, C.; Huo, D.; He, B.; Qian, L.; Fa, H. A high–selectivity electrochemical sensor for ultra-trace lead (II) detection based on a nanocomposite consisting of nitrogen-doped graphene/gold nanoparticles functionalized with ETBD and $Fe_3O_4@TiO_2$ core–shell nanoparticles. *Sens. Actuators B Chem.* **2017**, *242*, 889–896.

31. Tao, L.; Lou, Y.; Zhao, Y.; Hao, M.; Yang, Y.; Xiao, Y.; Tsang, Y.; Li, J. Silver nanoparticle-decorated graphene oxide for surface-enhanced Raman scattering detection and optical limiting applications. *J. Mater. Sci.* **2018**, *53*, 573–580. [CrossRef]

32. Wang, F.; Gu, Z.; Lei, W.; Wang, W.; Xia, X.; Hao, Q. Graphene quantum dots as a fluorescent sensing platform for highly efficient detection of copper(II) ions. *Sens. Actuators B Chem.* **2014**, *190*, 516–522. [CrossRef]

33. Li, J.; Wang, Z.; Yang, J.; Xia, X.; Yi, R.; Jiang, J.; Liu, W.; Chen, J.; Chen, L.; Xu, J. "On-off-on" fluorescence switch of graphene quantum dots: A cationic control strategy. *Appl. Surf. Sci.* **2021**, *546*, 149110. [CrossRef]

34. Zhu, S.; Tang, S.; Zhang, J.; Yang, B. Control the size and surface chemistry of graphene for the rising fluorescent materials. *Chem. Commun.* **2012**, *48*, 4527–4539. [CrossRef]

35. Zhao, G.; Li, J.; Ren, X.; Chen, C.; Wang, X. Few-layered graphene oxide nanosheets as superior sorbents for heavy metal ion pollution management. *Environ. Sci. Technol.* **2011**, *45*, 10454–10462. [CrossRef]

36. Chen, D.; Feng, H.; Li, J. Graphene oxide: Preparation, functionalization, and electrochemical applications. *Chem. Rev.* **2012**, *112*, 6027–6053. [CrossRef]

37. Coroş, M.; Pruneanu, S.; Stefan-van Staden, R.-I. Review—Recent Progress in the Graphene-Based Electrochemical Sensors and Biosensors. *J. ElectroChem. Soc.* **2020**, *167*, 037528. [CrossRef]

38. Jose, J.; Prakash, P.; Jeyaprabha, B.; Abraham, R.; Mathew, R.; Zacharia, E.; Thomas, V.; Thomas, J. Principle, design, strategies, and future perspectives of heavy metal ion detection using carbon nanomaterial-based electrochemical sensors: A review. *J. Iran. Chem. Soc.* **2023**, *20*, 775–791. [CrossRef]

39. Yang, J.; Maulik, G.; He, S.; Nag, A.; Deng, S.; Afsarimanesh, N.; Gao, J. Graphene allotropes-based electrochemical sensors to detect catechol molecules. *Sens. Actuators A Phys.* **2024**, *368*, 115088. [CrossRef]

40. Kumunda, C.; Adekunle, A.S.; Mamba, B.B.; Hlongwa, N.; Nkambule, T. Electrochemical Detection of Environmental Pollutants Based on Graphene Derivatives: A Review. *Front. Mater.* **2021**, *7*, 616787. [CrossRef]

41. Zuo, Y.; Xu, J.; Zhu, X.; Duan, X.; Lu, L.; Yu, Y. Graphene-derived nanomaterials as recognition elements for electrochemical determination of heavy metal ions: A review. *Microchim. Acta* **2019**, *186*, 171–186. [CrossRef]

42. Ali, Z.; Ullah, R.; Tuzen, M.; Ullah, S.; Rahim, A.; Saleh, T. Colorimetric sensing of heavy metals on metal doped metal oxide nanocomposites: A review. *Trends Environ. Anal. Chem.* **2023**, *37*, e00187. [CrossRef]

43. Fu, Q.; Bao, X. Surface chemistry and catalysis confined under two-dimensional materials. *Chem. Soc. Rev.* **2017**, *46*, 1842–1874. [CrossRef] [PubMed]

44. Falina, S.; Syamsul, M.; Rhaffor, N.A.; Sal Hamid, S.; Mohamed Zain, K.; Abd Manaf, A.; Kawarada, H. Ten years progress of electrical detection of heavy metal ions (Hmis) using various field-effect transistor (fet) nanosensors: A review. *Biosensors* **2021**, *11*, 478. [CrossRef]

45. Shao, Y.; Wang, J.; Wu, H.; Liu, J.; Aksay, I.; Lin, Y. Graphene based electrochemical sensors and biosensors: A review. *Electroanalysis* **2010**, *22*, 1027–1036. [CrossRef]

46. Chang, H.; Wu, H. Graphene-based nanocomposites: Preparation, functionalization, and energy and environmental applications. *Energy Environ. Sci.* **2013**, *6*, 3483–3507. [CrossRef]

47. Gahrouei, A.E.; Rezapour, A.; Pirooz, M.; Pourebrahimi, S. From classic to cutting-edge solutions: A comprehensive review of materials and methods for heavy metal removal from water environments. *Desalination Water Treat.* **2024**, *319*, 100446. [CrossRef]

48. Peng, H.; Guo, J. Removal of chromium from wastewater by membrane filtration, chemical precipitation, ion exchange, adsorption electrocoagulation, electrochemical reduction, electrodialysis, electrodeionization, photocatalysis and nanotechnology: A review. *Environ. Chem. Lett.* **2020**, *18*, 2055–2068. [CrossRef]

49. Ezugbe, E.O.; Rathilal, S. Membrane technologies in wastewater treatment: A review. *Membranes* **2020**, *10*, 89. [CrossRef] [PubMed]

50. Xiang, H.; Min, X.; Tang, C.J.; Sillanpää, M.; Zhao, F. Recent advances in membrane filtration for heavy metal removal from wastewater: A mini review. *J. Water Process Eng.* **2022**, *49*, 103–127. [CrossRef]

51. Zheng, B.; Tian, Y.; Jia, S.; Zhao, X.; Li, H. Molecular dynamics study on applying layered graphene oxide membranes for separating cadmium ions from water. *J. Membr. Sci.* **2020**, *603*, 1179–1196. [CrossRef]

52. Kim, I.S.; Hwang, M.; Choi, C. Membrane-Based Desalination Technology for Energy Efficiency and Cost Reduction. In *Desalination Sustainability: A Technical, Socioeconomic, and Environmental Approach*; Elsevier: Amsterdam, The Netherlands, 2017; pp. 31–74.

53. Li, Y.; Xu, Z.; Liu, S.; Zhang, J.; Yang, X. Molecular simulation of reverse osmosis for heavy metal ions using functionalized nanoporous graphenes. *Comput. Mater. Sci.* **2017**, *139*, 65–74. [CrossRef]

54. Cohen-Tanugi, D. Nanoporous Graphene as a Water Desalination Membrane. Ph.D. Thesis, Massachusetts Institute of Technology, Cambridge, MA, USA, 2012.

55. Yang, F.; Du, M.; Yin, K.; Qiu, Z.; Zhao, J.; Liu, C.; Zhang, G.; Gao, Y.; Pang, H. Applications of Metal-Organic Frameworks in Water Treatment: A Review. *Small* **2022**, *18*, 2105715. [CrossRef]

56. Velarde, L.; Nabavi, M.S.; Escalera, E.; Antti, M.; Akhtar, F. Adsorption of heavy metals on natural zeolites: A review. *Chemosphere* **2023**, *328*, 138508. [CrossRef] [PubMed]

57. Ali, A.; Ahmed, A.; Gad, A. Chemical and microstructural analyses for heavy metals removal from water media by ceramic membrane filtration. *Water Sci. Technol.* **2017**, *75*, 439–450. [CrossRef] [PubMed]

58. Nasrollahzadeh, M.; Sajjadi, M.; Iravani, S.; Varma, R. Carbon-based sustainable nanomaterials for water treatment: State-of-art and future perspectives. *Chemosphere* **2021**, *263*, 128005. [CrossRef] [PubMed]

59. Lei, Y.; Zhang, T.; Lin, Y.C.; Granzier-Nakajima, T.; Bepete, G.; Kowalczyk, D.; Lin, Z.; Zhou, D.; Schranghamer, T.; Dodda, A. Graphene and Beyond: Recent Advances in Two-Dimensional Materials Synthesis, Properties, and Devices. *ACS Nanosci. Au* **2022**, *2*, 450–485. [CrossRef] [PubMed]

60. Balandin, A.A.; Ghosh, S.; Bao, W.; Calizo, I.; Teweldebrhan, D.; Miao, F.; Lau, C. Superior thermal conductivity of single-layer graphene. *Nano Lett.* **2008**, *8*, 902–907. [CrossRef] [PubMed]

61. Gara, J.S.; Hubbard, W.; Reina, A.; Kong, J.; Branton, D.; Golovchenko, J.A. Graphene as a subnanometre trans-electrode membrane. *Nature* **2010**, *467*, 190–193. [CrossRef] [PubMed]

62. Bieri, M.; Treier, M.; Cai, J.; Aït-Mansour, K.; Ruffieux, P.; Gröning, O.; Gröning, P.; Kastler, M.; Rieger, R.; Feng, X. Porous graphenes: Two-dimensional polymer synthesis with atomic precision. *Chem. Commun.* **2009**, *45*, 6919–6921. [CrossRef]

63. Lemme, M.C.; Bell, D.C.; Williams, J.R.; Stern, L.A.; Baugher, B.; Jarillo-Herrero, P.; Marcus, C.M. Etching of graphene devices with a helium ion beam. *ACS Nano* **2009**, *3*, 2674–2676. [CrossRef] [PubMed]

64. Kim, M.; Safron, N.S.; Han, E.; Arnold, M.; Gopalan, P. Fabrication and characterization of large-area, semiconducting nanoperforated graphene materials. *Nano Lett.* **2010**, *10*, 1125–1131. [CrossRef] [PubMed]

65. Zeng, X.; Teng, J.; Yu, J.G.; Tan, A.S.; Fu, D.F.; Zhang, H. Fabrication of homogeneously dispersed graphene/Al composites by solution mixing and powder metallurgy. *Int. J. Miner. Metall. Mater.* **2018**, *25*, 102–109. [CrossRef]

66. Bell, N.J.; Ng, Y.H.; Du, A.; Coster, H.; Smith, S.; Amal, R. Understanding the enhancement in photoelectrochemical properties of photocatalytically prepared TiO2-reduced graphene oxide composite. *J. Phys. Chem. C* **2011**, *115*, 6004–6009. [CrossRef]

67. Georgakilas, V.; Otyepka, M.; Bourlinos, A.B.; Chandra, V.; Kim, N.; Kemp, K.C.; Hobza, P.; Zboril, R.; Kim, K. Functionalization of graphene: Covalent and non-covalent approaches, derivatives and applications. *Chem. Rev.* **2012**, *112*, 6156–6214. [CrossRef]

68. Mao, H.N.; Wang, X.G. Use of in-situ polymerization in the preparation of graphene/polymer nanocomposites. *Xinxing Tan Cailiao/New Carbon Mater.* **2020**, *35*, 336–343. [CrossRef]

69. Lee, S.J.; Yoon, S.J.; Jeon, I.Y. Graphene/Polymer Nanocomposites: Preparation, Mechanical Properties, and Application. *Polymers* **2022**, *14*, 4733. [CrossRef] [PubMed]

70. Talapatra, A.; Datta, D. A review of the mechanical, thermal and tribological properties of graphene reinforced polymer nanocomposites: A molecular dynamics simulations methods. *Polym. Bull.* **2023**, *80*, 2299–2328. [CrossRef]

71. Kim, K.S.; Zhao, Y.; Jang, H.; Lee, S.Y.; Kim, J.M.; Kim, K.S.; Ahn, J.-H.; Kim, P.; Choi, J.-Y.; Hong, B.H. Large-scale pattern growth of graphene films for stretchable transparent electrodes. *Nature* **2009**, *457*, 706–710. [CrossRef]

72. Qing, F.; Hou, Y.; Stehle, R.; Li, X. Chemical vapor deposition synthesis of graphene films. *APL Mater.* **2019**, *7*, 020903. [CrossRef]

73. Han, W.; Liu, L.; Yu, B.; Zhu, Q. Electrodeposition of graphene oxide-hydroxyapatite composite coating on titanium substrate. *Ceram Int.* **2023**, *49*, 9647–9656. [CrossRef]

74. Iqbal, M.S.; Aslam, A.A.; Iftikhar, R.; Ziegler, K.; Chakraborty, T. The potential of functionalized graphene-based composites for removing heavy metals and organic pollutants. *J. Water Process Eng.* **2023**, *53*, 103809. [CrossRef]

75. Sreeprasad, T.S.; Maliyekkal, S.M.; Lisha, K.P.; Pradeep, T. Reduced graphene oxide-metal/metal oxide composites: Facile synthesis and application in water purification. *J. Hazard. Mater.* **2011**, *186*, 921–931. [CrossRef] [PubMed]

76. Gkika, D.A.; Karmali, V.; Lambropoulou, D.A.; Mitropoulos, A.C.; Kyzas, G.Z. Membranes Coated with Graphene-Based Materials: A Review. *Membranes* **2023**, *13*, 127. [CrossRef]

77. Kumar, A.; Sharma, K.; Dixit, A.R. A review of the mechanical and thermal properties of graphene and its hybrid polymer nanocomposites for structural applications. *J. Mater. Sci.* **2019**, *54*, 5992–6026. [CrossRef]

78. Kumar, A.; Sharma, K.; Dixit, A.R. Carbon nanotube- and graphene-reinforced multiphase polymeric composites: Review on their properties and applications. *J. Mater. Sci.* **2020**, *55*, 2682–2724. [CrossRef]

79. Warsinger, D.M.; Chakraborty, S.; Tow, E.W.; Plumlee, M.H.; Bellona, C.; Loutatidou, S.; Karimi, L.; Mikelonis, A.M.; Achilli, A.; Ghassemi, A. A review of polymeric membranes and processes for potable water reuse. *Prog. Polym. Sci.* **2018**, *81*, 209–237. [CrossRef]

80. Alyarnezhad, S.; Marino, T.; Parsa, J.B.; Galiano, F.; Ursino, C.; Garcìa, H.; Puche, M.; Figoli, A. Polyvinylidene fluoride-graphene oxide membranes for dye removal under visible light irradiation. *Polymers* **2020**, *12*, 1509. [CrossRef] [PubMed]

81. Keirouz, A.; Galiano, F.; Russo, F.; Fontananova, E.; Castro-Dominguez, B.; Figoli, A.; Mattia, D.; Leese, H. Cyrene-Enabled Green Electrospinning of Nanofibrous Graphene-Based Membranes for Water Desalination via Membrane Distillation. *ACS Sustain. Chem. Eng.* **2024**, *12*, 17713–17725. [CrossRef] [PubMed]

82. Lou, M.; Li, J.; Zhu, X.; Chen, J.; Zhang, X.; Fang, X.; Li, F. Difunctional MOF-wrapped graphene membranes for efficient photothermal membrane distillation and VOCs interception. *J. Membr. Sci.* **2023**, *676*, 121592. [CrossRef]

83. Sera, J.S.; Mohammadi, T.; Tofighy, M.A. Graphene-based membranes for membrane distillation applications: A review. *J. Environ. Chem. Eng.* **2022**, *10*, 107974. [CrossRef]

84. Aquino, M.; Santoro, S.; Politano, A.; D'Andrea, G.; Siciliano, A.; Straface, S.; La Russa, M.F.; Curcio, E. Environmentally Friendly Photothermal Membranes for Halite Recovery from Reverse Osmosis Brine via Solar-Driven Membrane Crystallization. *Membranes* **2024**, *14*, 87. [CrossRef] [PubMed]

85. Rao, Z.; Feng, K.; Tang, B.; Wu, P. Surface decoration of amino-functionalized metal-organic framework/graphene oxide composite onto polydopamine-coated membrane substrate for highly efficient heavy metal removal. *ACS Appl. Mater. Interfaces* **2017**, *9*, 2594–2605. [CrossRef] [PubMed]

86. Zhang, P.; Gong, J.L.; Zeng, G.M.; An, Q.F.; Liu, Y.L.; Zhang, Y.M.; Hu, C.C.; Lee, K.R.; Lai, J.Y. Cross-linking to prepare composite graphene oxide-framework membranes with high-flux for dyes and heavy metal ions removal. *Chem. Eng. J.* **2017**, *322*, 657–666. [CrossRef]

87. Shukla, A.K.; Alam, J.; Alhoshan, M. Removal of heavy metal ions using a carboxylated graphene oxide-incorporated polyphenyl-sulfone nanofiltration membrane. *Environ. Sci.* **2018**, *4*, 438–448. [CrossRef]

88. Liu, W.; Wang, D.; Soomro, R.A.; Fu, F.; Qiao, N.; Yu, Y.; Wang, R.; Xu, B. Ceramic supported attapulgite-graphene oxide composite membrane for efficient removal of heavy metal contamination. *J. Membr. Sci.* **2019**, *591*, 117323. [CrossRef]

89. Zhang, Y.; Zhang, S.; Chung, T.S. Nanometric Graphene Oxide Framework Membranes with Enhanced Heavy Metal Removal via Nanofiltration. *Environ. Sci. Technol.* **2015**, *49*, 10235–10242. [CrossRef]

90. Zhang, Y.; Zhang, S.; Gao, J.; Chung, T.S. Layer-by-layer construction of graphene oxide (GO) framework composite membranes for highly efficient heavy metal removal. *J. Membr. Sci.* **2016**, *515*, 230–237. [CrossRef]

91. Abdi, G.; Alizadeh, A.; Zinadini, S.; Moradi, G. Removal of dye and heavy metal ion using a novel synthetic polyethersulfone nanofiltration membrane modified by magnetic graphene oxide/metformin hybrid. *J. Membr. Sci.* **2018**, *552*, 326–335. [CrossRef]

92. Malik, L.A.; Bashir, A.; Qureashi, A.; Pandith, A.H. Detection and removal of heavy metal ions: A review. *Environ. Chem. Lett.* **2019**, *17*, 1495–1521. [CrossRef]

93. Qian, L.; Thiruppathi, A.R.; Van Der Zalm, J.; Chen, A. Graphene Oxide-Based Nanomaterials for the Electrochemical Sensing of Isoniazid. *ACS Appl. Nano Mater.* **2021**, *4*, 3696–3706. [CrossRef]

94. Kadhom, M.; Deng, B. Metal-organic frameworks (MOFs) in water filtration membranes for desalination and other applications. *Appl. Mater. Today* **2018**, *11*, 219–230. [CrossRef]

95. Kakar, U.M.; Tauanov, Z.; Azat, S.; Ahmadi, N.; Hassand, M.H.; Sarwari, A. Carbon Nanotubes as Adsorbents for Heavy Metals: Focus on Arsenic and Hydrargyrum Removal from Water. *J. Chem. Stud.* **2024**, *3*, 07–20. [CrossRef]

96. Han, Z.Y.; Huang, L.J.; Qu, H.J.; Wang, Y.; Zhang, Z.J.; Rong, Q.I.; Sang, Z.Q.; Wang, Y.; Kipper, M.J.; Tang, J.G. A review of performance improvement strategies for graphene oxide-based and graphene-based membranes in water treatment. *J. Mater. Sci.* **2021**, *56*, 9545–9574. [CrossRef]

97. Pan, B.; Yin, X.; Iglauer, S. A review on clay wettability: From experimental investigations to molecular dynamics simulations. *Adv. Colloid Interface Sci.* **2020**, *285*, 102266. [CrossRef]

98. Ghosh, S.; Sotskov, V.; Shapeev, A.V.; Neugebauer, J.; Körmann, F. Short-range order and phase stability of CrCoNi explored with machine learning potentials. *Phys. Rev. Mater.* **2022**, *6*, 113804. [CrossRef]

99. Sperger, T.; Sanhueza, I.A.; Schoenebeck, F. Computation and Experiment: A Powerful Combination to Understand and Predict Reactivities. *Acc. Chem. Res.* **2016**, *49*, 1311–1319. [CrossRef]

100. Samstag, R.W.; Ducoste, J.J.; Griborio, A.; Nopens, I.; Batstone, D.J.; Wicks, J.D.; Saunders, S.; Wicklein, E.A.; Kenny, G.; Laurent, J. CFD for wastewater treatment: An overview. *Water Sci. Technol.* **2016**, *74*, 549–563. [CrossRef] [PubMed]

101. Guediri, A.; Bouguettoucha, A.; Chebli, D.; Chafai, N.; Amrane, A. Molecular dynamic simulation and DFT computational studies on the adsorption performances of methylene blue in aqueous solutions by orange peel-modified phosphoric acid. *J. Mol. Struct.* **2020**, *1202*, 127290. [CrossRef]

102. Fakhari, S.M.; Mrad, H. Aerodynamic shape optimization of NACA airfoils based on a novel unconstrained conjugate gradient algorithm. *J. Eng. Res.* **2024**, *020*, 1–10. [CrossRef]

103. Macuglia, D. SHAKE and the exact constraint satisfaction of the dynamics of semi-rigid molecules in Cartesian coordinates, 1973–1977. *Arch. Hist. Exact. Sci.* **2023**, *77*, 345–371. [CrossRef]

104. Vzzlzrt, L. 'Exyeriments' on Classical Fluids. I. Thermodynamical Properties of Lennard,-Jones Molecules. *Phys. Rev.* **1967**, *159*, 98.

105. Hoover, W.G.; Holian, B.L. Kinetic moments method for the canonical ensemble distribution. *Phys. Lett. A* **1996**, *2*, 253–257. [CrossRef]

106. Hoover, W.G. Canonical dynamics: Equilibrium phase-space distributions. *Phys. Rev. A* **1985**, *31*, 94550–95554. [CrossRef]

107. Wang, S.; Maganga, I.; Zeng, L.; Gu, Z. Graphene crown pore for efficient heavy metal ion Removal: Protonated vs. Non-protonated. *J. Mol. Liq.* **2024**, *395*, 123819. [CrossRef]

108. Khalajiolyaie, A.; Jian, C. Advancing wastewater treatment from cadmium contamination via functionalized graphene nanosheets. *J. Water Process Eng.* **2024**, *63*, 105491. [CrossRef]

109. Azamat, J.; Khataee, A.; Joo, S.W. Functionalized graphene as a nanostructured membrane for removal of copper and mercury from aqueous solution: A molecular dynamics simulation study. *J. Mol. Graph. Model.* **2014**, *53*, 112–117. [CrossRef] [PubMed]

110. Majidi, S.; Erfan-Niya, H.; Azamat, J.; Cruz-Chú, E.R.; Walther, J.H. Efficient Removal of Heavy Metals from Aqueous Solutions through Functionalized γ-Graphyne-1 Membranes under External Uniform Electric Fields: Insights from Molecular Dynamics Simulations. *J. Phys. Chem. B* **2021**, *125*, 12254–12263. [CrossRef] [PubMed]

111. Hasanzadeh, A.; Alizadeh, M.; Ajalli, N.; Azamat, J.; Jahanshahi, M. Molecular dynamic simulation and artificial neural network (ANN) modeling of the functionalized graphene oxide membranes on Cr (VI) ion removal through electrodialysis method. *J. Mol. Liq.* **2023**, *383*, 122083. [CrossRef]

112. Rahiminejad, M.; Mortazavi, V.; Moosavi, A.; Nouri-Borujerdi, A. Transport of Water Contaminated with Various Ions Through Nanoporous Graphene: A Molecular Dynamics Simulation. *Transp. Porous Media* **2022**, *242*, 537–557. [CrossRef]

113. Tabasi, E.; Vafa, N.; Firoozabadi, B.; Salmankhani, A.; Nouranian, S.; Habibzadeh, S.; Mashhadzadeh, A.H.; Spitas, C.; Saeb, M. Ion rejection performances of functionalized porous graphene nanomembranes for wastewater purification: A molecular dynamics simulation study. *Colloids Surf. A Physicochem. Eng. Asp.* **2023**, *656*, 130492. [CrossRef]

114. Zheng, B.; Chu, X.; Li, H.; Wu, X.; Zhao, X.; Tian, Y. Layered graphene oxide membranes functioned by amino acids for efficient separation of metal ions. *Appl. Surf. Sci.* **2021**, *546*, 149145. [CrossRef]

115. Khalajiolyaie, A.; Jian, C. Mechanistic understanding of the functioning of two-layer graphene membranes at the nanoscale for wastewater treatment. *J. Mol. Liq.* **2025**, *420*, 126833. [CrossRef]

116. Zheng, B.; Chu, X.; Peng, Z.; Tian, Y. Improving the separation performance for heavy metals by optimizing the structure of multilayered GO membrane. *J. Mol. Liq.* **2023**, *370*, 1–11. [CrossRef]

117. Chen, Y.; Yang, X. Molecular simulation of layered GO membranes with amorphous structure for heavy metal ions separation. *J. Membr. Sci.* **2022**, *660*, 107947. [CrossRef]

118. Giri, A.K.; Cordeiro, M.N.D.S. Heavy metal ion separation from industrial wastewater using stacked graphene Membranes: A molecular dynamics simulation study. *J. Mol. Liq.* **2021**, *338*, 116688. [CrossRef]

119. Panahi, A.; Shomali, A.; Sabour, M.H.; Ghafar-Zadeh, E. Molecular dynamics simulation of electric field driven water and heavy metals transport through fluorinated carbon nanotubes. *J. Mol. Liq.* **2019**, *278*, 658–671. [CrossRef]

120. Chen, A.; Liu, W.; Soomro, R.A.; Wei, Y.; Zhu, X.; Qiao, N.; Kang, Y.; Xu, B. PVA-integrated graphene oxide-attapulgite composite membrane for efficient removal of heavy metal contaminants. *Environ. Sci. Pollut. Res.* **2022**, *29*, 84410–84420. [CrossRef] [PubMed]

121. Ercarikci, E.; Alanyalioglu, M. Dual-Functional Graphene-Based Flexible Material for Membrane Filtration and Electrochemical Sensing of Heavy Metal Ions. *IEEE Sens. J.* **2021**, *21*, 2468–2475. [CrossRef]

122. Lari, S.; Parsa, S.A.M.; Akbari, S.; Emadzadeh, D.; Lau, W.J. Fabrication and evaluation of nanofiltration membrane coated with amino-functionalized graphene oxide for highly efficient heavy metal removal. *Int. J. Environ. Sci. Tech.* **2022**, *19*, 4615–4626. [CrossRef]

123. Liu, Z.; Wang, Q.; Huang, X.; Qian, X. Surface Functionalization of Graphene Oxide with Hyperbranched Polyamide-Amine and Microcrystalline Cellulose for Efficient Adsorption of Heavy Metal Ions. *ACS Omega* **2022**, *7*, 10944–10954. [CrossRef] [PubMed]

124. Arvidsson, R. Review of environmental life cycle assessment studies of graphene production. *Adv. Mater. Lett.* **2017**, *8*, 187–195. [CrossRef]

125. Zaaba, N.I.; Foo, K.L.; Hashim, U.; Tan, S.J.; Liu, W.; Voon, C.H. Synthesis of Graphene Oxide using Modified Hummers Method: Solvent Influence. *Procedia Eng.* **2017**, *184*, 469–477. [CrossRef]

126. Li, X.; Jin, H.; Chan, Y.; Guo, H.; Ma, W. Environmental impacts of graphene at industrial production scale and its application in electric heating technology. *Resour. Conserv. Recycl.* **2023**, *199*, 1–10. [CrossRef]

127. Nayak, T.; Pathan, A. Environmental remediation and application of carbon-based nanomaterials in the treatment of heavy metal-contaminated water: A review. *Mater. Today Proc.* **2023**, *92*, 1659–1670. [CrossRef]

128. Abd Rahman, F.H.; Amiruddin, H.; Abdollah, M.F.B.; Mohd Zulkifli, N.; Samion, S.; Umehara, N.; Tanemura, M.; Honda, M.; Morina, A. Synthesising graphene with renewably-sourced bio-carbon precursors: A brief review. *J. Braz. Soc. Mech. Sci. Eng.* **2024**, *46*, 173–186. [CrossRef]

129. Kazemi, A.; Bahramifar, N.; Heydari, A.; Olsen, S. Life cycle assessment of nanoadsorbents at early stage technological development. *J. Clean. Prod.* **2018**, *174*, 527–537. [CrossRef]

130. Munuera, J.; Britnell, L.; Santoro, C.; Cuéllar, R.; Casiraghi, C. A review on sustainable production of graphene and related life cycle assessment. *2D Mater.* **2022**, *9*, 012002. [CrossRef]

131. Sulthana, S.F.; Iqbal, U.M.; Suseela, S.B.; Anbazhagan, R.; Chinthaginjala, R.; Chitathuru, D.; Ahmad, I.; Kim, T. Electrochemical Sensors for Heavy Metal Ion Detection in Aqueous Medium: A Systematic Review. *ACS Omega* **2024**, *9*, 25493–25512. [CrossRef] [PubMed]

132. McGarrity, M.; Zhao, F. Graphene-Based Chemiresistor Sensors for Drinking Water Quality Monitoring. *Sensors* **2023**, *23*, 9828. [CrossRef]

133. Saputra, H.A. Electrochemical sensors: Basic principles, engineering, and state of the art. *Monatsh Chem.* **2023**, *154*, 1083–1100. [CrossRef]

134. Dilshad, M.; Hussain, T.; Ali, S.; Shakeel, M.; Javed, M.; Nazir, F.; Ahmad, A. Graphene-Based Electrochemical Sensors for Heavy Metal Ions Detection: A Comprehensive Review. *ASEAN J. Sci. Eng. Mater.* **2025**, *4*, 23–42.

135. Atacan, K. $CuFe_2O_4$/reduced graphene oxide nanocomposite decorated with gold nanoparticles as a new electrochemical sensor material for L-cysteine detection. *J. Alloys. Compd.* **2019**, *791*, 391–401. [CrossRef]

136. Ayala-Claveria, M.; Carlesi, C.; Puig, J.; Olguin, G. The Impact of Adsorption Property Modification by Crosslinkers on Graphene Oxide Membrane Separation Performance. *Processes* **2024**, *12*, 2320. [CrossRef]

137. Guha, R.; Xiong, B.; Geitner, M.; Moore, T.; Wood, T.; Velegol, D.; Kumar, M. Reactive micromixing eliminates fouling and concentration polarization in reverse osmosis membranes. *J. Membr. Sci.* **2017**, *542*, 8–17. [CrossRef]

138. Tan, L.; Chen, Z.; Zhao, Y.; Wei, X.; Li, Y.; Zhang, C.; Wei, X.; Hu, X. Dual channel sensor for detection and discrimination of heavy metal ions based on colorimetric and fluorescence response of the AuNPs-DNA conjugates. *BioSens. Bioelectron.* **2016**, *85*, 414–421. [CrossRef]

139. Cohen-Tanugi, D. Nanoporous graphene as a water desalination membrane. *Technol. (Singap. World Sci.)* **2012**, *12*, 3602–3608.

140. Kang, J.W.; Hwang, H.J. Gigahertz actuator of multiwall carbon nanotube encapsulating metallic ions: Molecular dynamics simulations. *J. Appl. Phys.* **2004**, *96*, 3900–3905. [CrossRef]

141. Song, N.; Gao, X.; Ma, Z.; Wang, X.; Wei, Y.; Gao, C. A review of graphene-based separation membrane: Materials, characteristics, preparation and applications. *Desalination* **2018**, *437*, 59–72. [CrossRef]

142. Movaghgharnezhad, S.; Kang, P. Laser-induced graphene: Synthesis advances, structural tailoring, enhanced properties, and sensing applications. *J. Mater. Chem. C Mater.* **2024**, *12*, 6718–6742. [CrossRef]

143. Moon, H.R.; Ryu, B. Review of Laser-Induced Graphene (LIG) Produced on Eco-Friendly Substrates. *Int. J. Precis. Eng. Manuf.—Green Technol.* **2024**, *11*, 1279–1294. [CrossRef]

144. Kommu, A.; Singh, J.K. A review on graphene-based materials for removal of toxic pollutants from wastewater. *Soft. Mater.* **2020**, *18*, 297–322. [CrossRef]